

# 1 Proteomics Uncovers Immunosuppression in COVID-19

## 2 Patients with Long Disease Course

3 Shaohua Tang <sup>1#</sup>, Rui Sun <sup>2,3#</sup>, Qi Xiao <sup>2,3#</sup>, Tingting Mao <sup>1#</sup>, Weigang Ge <sup>2,3#</sup>, Chongquan  
4 Huang <sup>1#</sup>, Meng Luo <sup>2,3,4</sup>, Liujia Qian <sup>2,3</sup>, Hao Chen <sup>2,3</sup>, Qiushi Zhang <sup>2,3</sup>, Sainan Li <sup>2,3</sup>, Wei  
5 Liu <sup>2,3,5</sup>, Shufei Li <sup>1</sup>, Xueqin Xu <sup>1</sup>, Huanzheng Li <sup>1</sup>, Lianpeng Wu <sup>1</sup>, Jianyi Dai <sup>1</sup>, Huanhuan  
6 Gao <sup>2,3</sup>, Lu Li <sup>2,3</sup>, Tian Lu <sup>2,3</sup>, Xiao Liang <sup>2,3</sup>, Xue Cai <sup>2,3</sup>, Guan Ruan <sup>2,3</sup>, Kexin Liu <sup>4</sup>, Fei Xu <sup>5</sup>,  
7 Yan Li <sup>6</sup>, Yi Zhu <sup>2,3 \*</sup>, Jianping Huang <sup>1\*</sup>, Tiannan Guo <sup>2,3,7\*</sup>

8 <sup>1</sup> Wenzhou Central Hospital, Dingli Clinical Medical School of Wenzhou Medical University,  
9 Wenzhou, 325000, Zhejiang, China;

10 <sup>2</sup> Key Laboratory of Structural Biology of Zhejiang Province, School of Life Sciences, Westlake  
11 University, 18 Shilongshan Road, Hangzhou 310024, Zhejiang Province, China;

12 <sup>3</sup> Institute of Basic Medical Sciences, Westlake Institute for Advanced Study, 18 Shilongshan Road,  
13 Hangzhou 310024, Zhejiang Province, China;

14 <sup>4</sup> Department of Clinical Pharmacology, College of Pharmacy, Dalian Medical University, Dalian  
15 200335, Liaoning, China

16 <sup>5</sup> Department of Anatomy, College of Basic Medical, Dalian Medical University, Dalian, China

17 <sup>6</sup> Department of Anatomy and Physiology, College of Basic Medical Sciences, Shanghai Jiao Tong  
18 University, No.280 Chongqing South Road, Shanghai 200025, China

19 <sup>7</sup> Lead Contact

20 # These authors contribute equally

21 \* Correspondence: [zhuyi@westlake.edu.cn](mailto:zhuyi@westlake.edu.cn) (Y.Z.); [hjpxzyy006@163.com](mailto:hjpxzyy006@163.com) (J.H.); [guotiannan@westlake.edu.cn](mailto:guotiannan@westlake.edu.cn)  
22 (T.G.)

## 24 Abstract

25 Little is known regarding why a subset of COVID-19 patients exhibited  
26 prolonged positivity of SARS-CoV-2 infection. Here, we studied the sera proteomic  
27 dynamics in 37 COVID-19 patients over nine weeks, quantifying 2700 proteins with  
28 high quality. Remarkably, we found that during the first three weeks since disease  
29 onset, while clinical symptoms and outcome were indistinguishable, patients with  
30 prolonged disease course displayed characteristic immunological responses including  
31 enhanced Natural Killer cell-mediated innate immunity and regulatory T cell-  
32 mediated immunosuppression. We further showed that it is possible to predict the  
33 length of disease course using machine learning based on blood protein levels during  
34 the first three weeks. Validation in an independent cohort achieved an accuracy of  
35 82%. In summary, this study presents a rich serum proteomic resource to understand  
36 host responses in COVID-19 patients and identifies characteristic Treg-mediated  
37 immunosuppression in patients with prolonged disease course, nominating new  
38 therapeutic target and diagnosis strategy.

39  
**NOTE: This preprint reports new research that has not been certified by peer review and should not be used to guide clinical practice.**

## 40 INTRODUCTION

41 COVID-19 caused by the SARS-CoV-2 virus is an ongoing pandemic spreading  
42 all over the world. About 80% of COVID-19 patients exhibit mild clinical symptoms  
43 including fever and cough, while ~20% of patients deteriorate to life-threatening  
44 severe or critical conditions (Wu and McGoogan, 2020). Multiple studies have  
45 investigated the clinical course and pathogenesis (To et al., 2020; Yang et al., 2020;  
46 Zhou et al., 2020) and molecular changes (Messner, 2020; Shen, 2020; Wu et al.,  
47 2020) of severe or critical cases.

48 What remains largely unknown is the substantial diversity of COVID-19 patients  
49 in terms of disease course. In a recent report, the median interval of COVID-19  
50 patients from onset to clinical recovery was 20 days, with the longest disease course  
51 of 37 days (Zhou et al., 2020). According to our clinical treatment of 37 COVID-19  
52 patients, some patients exhibited surprisingly prolonged virus infection. The longest  
53 disease course we have observed thus far is 107 days (P33, a 55-year-old male) as of  
54 17 May 2020. Little is known about the causes of persistent virus infection and how  
55 he could be effectively treated.

56 Here we report a longitudinal and in-depth proteomic profiling of 37 COVID-19  
57 patients with short and long disease courses. We analyzed the sera proteomes  
58 collected over nine weeks for both patients with short disease course (SC) who turned  
59 negative for the virus infection in less than 22 days, and patients with long disease  
60 course (LC) who remained positive for 22 days or longer. We have also analyzed the  
61 sera proteomes of 35 non-COVID-19 patients with flu-like symptoms as controls.  
62 2700 proteins were quantified with high quality, offering a rich resource to understand  
63 the dynamic disease course of COVID-19 patients in response to virus infection. Our  
64 data showed characteristic immune responses between the SC and LC patient groups.  
65 Remarkably, the data suggest regulatory T cell (Treg)-mediated immunosuppression  
66 was specifically activated in LC patients. We also showed that it is possible to predict  
67 the disease course of COVID-19 patients by measuring the characteristic protein  
68 levels from blood samples collected in the first three weeks since disease onset using  
69 a machine learning model. This study not only presents a rich resource to study the  
70 COVID-19 host responses, but also nominates novel therapeutic and diagnostic  
71 strategies for COVID-19 patients with prolonged infection positivity.

## 73 RESULTS AND DISCUSSION

### 74 Patients, samples and proteomics

75 We procured 37 COVID-19 patients in this study of which 35 were typical and  
76 two were severe cases (Table 1, Table S1), including 19 males and 18 females, with a  
77 median age of 48 years. The median duration of disease in this cohort, as defined in  
78 Methods, was 22 days. These patients were divided into two groups based on the  
79 length of their disease course (Figure 1). The SC group comprised 17 patients with a  
80 disease course shorter than 22 days. The other 20 patients were defined as LC group.  
81 Interestingly, one of the severe cases was classified as SC, while the other severe case

82 was in the LC group (Figure 1).

83 These two groups (SC and LC) were indistinguishable based on clinical  
84 symptoms. The median age of SC patients was 43.2 years (range, 27-67 years) for SC  
85 patients, and 49.0 years (range, 2-84 years) for LC patients. The Wilcoxon t-test showed  
86 no significant age difference between the SC and LC patient groups (Figure S1A).  
87 Clinical treatment of both groups of patients was not significantly different by  
88 Fisher's exact test (Figure S1B, Table 1), indicating that the different lengths of  
89 disease course were unlikely due to existing therapeutics. Routine blood test data for  
90 the two groups showed no significant difference either (Figure S1C). We analyzed an  
91 additional 35 non-COVID-19 patients with flu-like symptoms as controls (Table 1,  
92 Table S1, and Figure 1B).

93 We performed in-depth profiling for sera proteome collected from each patient  
94 over nine weeks using TMTpro 16plex-based data-dependent acquisition mass  
95 spectrometry (Thompson et al., 2019). 14 high-abundance blood proteins were largely  
96 depleted to enhance the ability to measure low-abundance proteins. Each TMT-  
97 labeled peptide mixture was fractionated into 26-30 fractions for comprehensive  
98 discovery proteomic analysis (Figure 1A). A total of 224 depleted serum samples  
99 were analyzed using TMT-based proteomics (Figure 1). Samples were randomly  
100 distributed into 18 batches. We also analyzed 44 technical replicates for randomly  
101 selected samples in each batch (Figure S2A). Each pool of TMT-labeled peptides was  
102 further fractionated into 26-30 fractions using high-pH reverse phase liquid  
103 chromatography (RPLC) and analyzed by LC-MS/MS using a 60-min RPLC gradient.  
104 The median coefficient of variance (CV) among MS/MS technical replicates was 0.19  
105 (Figure S2B). After excluding proteins with missing values in over 80% of samples,  
106 we presented quantitative levels of 2700 proteins across 268 sera samples with  
107 relatively high degrees of quantitative accuracy (Table S2A).

108

### 109 **Complex immunity in the LC patients**

110 To investigate host response differences in the serum proteome data set from the  
111 SC and LC patients, we performed a pairwise comparison of the proteins quantified in  
112 these two groups at each week over nine weeks. We then combined the regulated  
113 proteins at each week, leading to the identification of 921 dysregulated proteins  
114 (Table S2B), of which 405 proteins were functionally annotated in the UniProt  
115 database. We firstly used only GO biological process, KEGG and Reactome pathway  
116 enrichment using 405 proteins, and found that most pathways were related to  
117 immunity and metabolism (Figure S3).

118 Generally, our data showed that the first week is the inflammatory response  
119 period, featured by activation of redox and amino acid metabolic processes. In the  
120 following three weeks, more pathways involved in adaptive immunity and  
121 glycometabolism were activated. Interestingly, some sex hormone associated  
122 pathways were also enriched, such as fertilization and response to estradiol. From  
123 fifth to ninth week, the two patient groups displayed difference in pathways involved  
124 in tissue remodelling and repair, apoptosis and sulfur compound catabolic process.

125 We then focused on the immunity-related pathways at each time point as shown

126 in Figure 2A. For SC patients, they showed upregulated platelet degranulation in the  
127 first week, followed by activation of antigen presentation in the following two weeks.  
128 Leukocyte degranulation was activated in the third week. In the sixth week, SC  
129 patients showed upregulation of serum proteins involved in tissue remodeling (Figure  
130 2A) as signs of recovery. LC patients displayed much more complex serum proteome  
131 dynamics. During the first week, both platelet degranulation and upregulation of Treg  
132 vs Teff were activated. Activation of antigen presentation occurred in the second  
133 week. The complement system was also activated from the second week.  
134 Interestingly, the regulatory T cell (Treg) activation pathway was enriched in the first  
135 two weeks and the fifth week, suggesting immunosuppression occurred early in these  
136 patients. From the fourth week, leukocyte migration was enriched. Tissue repair was  
137 enriched only in the eighth week, followed by the complement system in the ninth  
138 week (Figure 2A). These data suggest that immunological responses during the first  
139 three weeks may be critical in determining the length of the disease course. During  
140 this period, both innate and adaptive immunity were activated in SC patients, while in  
141 contrast, LC patients showed signs of Treg-mediated immunosuppression in addition  
142 to innate and adaptive immunity.

143 Our data also underscored the proteins involved in the above-mentioned  
144 pathways as shown in Figure S3. In SC patients, a secreted protein, the soluble  
145 scavenger receptor cysteine-rich domain-containing protein (SSC5D) was highly  
146 expressed in the second week (Figure S4). SSC5D is highly expressed on monocytes  
147 and activated lymphocytes rather than naïve immune cells, and mediates both innate  
148 and adaptive immunity (Goncalves et al., 2009), suggesting activated immune  
149 responses to virus infection. In the third week, another upregulated protein in SC  
150 patient sera was non-secretory ribonuclease (RNASE2), a chemoattractant for  
151 dendritic cells. RNASE2 is reported to participate in antigen presentation (Yang et al.,  
152 2003), and may play a role in the adaptive immunity against SARS-CoV-2 (Figure  
153 S4). In the fourth week, a pro-inflammatory factor, chromogranin-A (CHGA), was  
154 upregulated in the sera in SC patients. CHGA highly expressed on the secretory cells  
155 to regulate catecholamine secretion which is associated with serum CHGA (di Comite  
156 et al., 2006) and is reported to activate pro-inflammatory M1 macrophages and inhibit  
157 anti-inflammatory M2 macrophages (Eissa et al., 2018). In the sixth week, serum  
158 amyloid P-component (APCS) was upregulated in SC patient sera (Figure S4),  
159 suggesting clearance of damaged circulating cells and enhanced angiogenesis.

160 In LC patients, positive regulators for immune response were found to be  
161 activated. Hepatocyte growth factor-like protein (MST1) was upregulated in the  
162 second week (Figure 2A). MST1 is required for thymocyte migration and antigen  
163 recognition (Ueda et al., 2012). Besides, Golgi-associated plant pathogenesis related  
164 protein 2 (GLIPR2), associated with the migration of T and B lymphocytes, was up-  
165 regulated in the fourth week (Figure S4). In the following week, we observed  
166 upregulation of two immunosuppressive factors, namely fibroleukin (FGL2) and  
167 programmed cell death 1 ligand 2 (PDCD1LG2). FGL2 negatively regulates dendritic  
168 cell antigen presentation and T cell differentiation, especially the secreted FGL2 (Hu  
169 et al., 2016). It was upregulated in LC patients and further increased during recovery

170 from COVID-19 (Figure S4). PDCD1LG2 negatively regulates T cell activation  
171 (Brown et al., 2003), and followed similar dynamics over the disease course to FGL2  
172 (Figure S4). In the eighth week, tissue remodeling associated proteins, such as von  
173 Willebrand factor (VWF), were upregulated in the LC group, suggesting recovery  
174 from COVID-19. Besides, our data show that the complement system may play  
175 important roles in LC patients during the entire disease course. In the second week,  
176 the most enriched pathway involving the upregulation of C5 was the complement  
177 cascade (Figure 2A). In the last week, C8A and other complement system proteins  
178 remained upregulated (Figure S4). Complement activation was reported in our  
179 previous study of COVID-19 sera (Shen, 2020). The complement cascade could also  
180 contribute to immunosuppression (Kemper et al., 2003) and might be a potential  
181 therapeutic target for COVID-19 (Cao, 2020).

182 Altogether, negative regulator factors and innate immune performed more active  
183 might result in longer disease course.

184

### 185 **Characteristic protein dynamics in the LC patients**

186 Next, we investigated whether the differentially expressed proteins between SC  
187 and LC patients were unique to COVID-19 disease by making comparison between  
188 COVID-19 and non-COVID-19 patients with flu-like symptoms (Ctrl, Figure 1B). We  
189 first analyzed the temporal dynamics of the 2700 proteins using Mfuzz (Kumar and  
190 Mattias, 2007) for SC and LC patients. 1746 proteins, grouped in eight clusters in the  
191 SC and LC patient groups (Table S2C), were consistently dysregulated over time  
192 compared to the control group (Figure S5A-B). Four characteristic protein clusters  
193 were enriched in the two patient groups (Figure S5C). In the meantime, 774 proteins  
194 were identified to be differentially expressed in COVID-19 patients compared to the  
195 Ctrl group (Table S2D). By overlapping the two above-mentioned protein shortlists  
196 with the 921 dysregulated proteins between SC and LC patients, our data were  
197 narrowed down to 207 proteins which fulfill the following three criteria: a)  
198 differentially expressed between SC and LC; b) consistently up- or down-regulated  
199 over time; c) COVID-19 disease specific (Figure 2B). Out of 207 proteins, 97 proteins  
200 were functionally annotated by the Ingenuity Pathway Analysis (IPA) software tool  
201 (Table S2E).

202 These proteins were segregated into two major groups based on their expression  
203 across all nine time points during the disease course (Figure 2C). The first group of 80  
204 proteins showed increased expression over time. SC patients exhibited earlier  
205 elevation of these proteins, while LC patients exhibited delayed increase (Figure 2C).  
206 Four major pathways were enriched in this protein group, namely acute phase  
207 response, LXR/RXR activation, agranulocyte adhesion and diapedesis, and actin  
208 cytoskeleton signaling (Figure 2D). Also, the coagulation and complement systems  
209 were also enriched in this protein group. Acute phase response signaling, coagulation  
210 and complement systems are associated with innate immunity, while actin  
211 cytoskeleton signaling is associated with leukocyte migration in adaptive immunity.

212 The second group of 17 proteins showed decreasing expression over time. SC  
213 patients showed an earlier decrease than LC patients (Figure 2E). These proteins were



214 mapped to enriched pathways including metabolic processes such as myo-inositol  
215 biosynthesis, glycolytic shunt and glutamyl cycle (Figure 2E).

216 Next, we calculated the median expression level of the two groups of proteins and  
217 present them in boxplots (Figure 2D, 2E). For the first group of proteins, generally SC  
218 patients showed lower protein expression than LC patients in the first three weeks, but  
219 the expression was dramatically elevated from the fourth week and maintained  
220 thereafter at a high level for several weeks (Figure 3D). This agrees with clinical data  
221 that all these SC patients tested negative for SARS-CoV-2 nucleic acid after the third  
222 week. In contrast, LC patients showed a higher degree of longitudinal diversity in the  
223 trends of expression of these proteins, probably partly due to their variable clinical  
224 recovery trajectories. Expression of the first group of proteins in the first four weeks  
225 was relatively stable but dramatically increased in the fifth week, followed by a  
226 decrease from the sixth to the seventh week, and a second rise in the eighth week  
227 (Figure 2D).

228 Interestingly, the expression of the second group of proteins displayed an  
229 opposite trend compared to the first group (Figure 2E). Protein expression of the SC  
230 patients started to decrease during the 4<sup>th</sup> week and continued to decrease until the last  
231 time point; while the LC patients showed high protein expression level till the fifth  
232 week, with a shallow decrease beginning in the sixth week (Figure 2E).

233

### 234 **Dysregulated leukocyte migration and IFG/redox homeostasis**

235 Pathway analysis of the two protein groups mentioned above highlighted  
236 leukocyte migration and IGF/redox homeostasis (Figure 3).

237 Representative proteins related to leukocyte migration included beta-defensin 1  
238 (DEFB1), selectin P (SELP), ezrin (EZR) and moesin (MSN) (Figure 3A). DEFB1 is  
239 a ligand for the chemokine receptor CCR6 and a positive upstream regulator of Th17  
240 (Wojtowicz et al., 2015). SC patients exhibited high expression of DEFB1 in the first  
241 three weeks, but it decreased from the fourth week when patients became negative in  
242 the nucleic acid test (Figure 3A). In contrast, LC patients exhibited a delayed increase  
243 of this protein until the third week (Figure 3A), suggesting delayed activation of Th17  
244 in LC patients. Leukocyte extravasation occurs in two sequential steps, among which  
245 SELP participates in the first process of leukocyte adhesion to the endothelial surface  
246 (Vicente-Manzanares and Sanchez-Madrid, 2004). In SC patients, expression of SELP  
247 was relatively low in the first three weeks, and then increased significantly in the  
248 fourth week and maintained at a high level until the ninth week (Figure 3A). SELP  
249 increase in LC patients, however, was much shallower, and peaked as late as the  
250 eighth week, in line with their prolonged disease course (Figure 3A). The complex of  
251 ezrin-radixin-moesin (ERM) links cytoskeleton with membrane adhesion molecules;  
252 however, moesin (MSN) and ezrin exert opposite functions (Ivetic et al., 2002). Our  
253 data showed that EZR was maintained at a relatively high level during the first three  
254 weeks in SC patients and then decreased thereafter (Figure 3A). Interestingly, in these  
255 patients, MSN showed an opposite trend in which expression increased from the  
256 fourth week and thereafter was maintained at a relatively high level. In LC patients,  
257 the change of ERM components showed a similar pattern but with a delayed transition

258 point (Figure 3A).

259 In addition to the proteins directly involved in immunity, our data also  
260 highlighted metabolic pathways such as the IGF/redox homeostasis pathway which is  
261 critical in maintaining the microenvironment for immune responses (Figure 3A). We  
262 narrowed our focus to proteins involved in IGF/redox homeostasis namely insulin-like  
263 growth factor 1 (IGF1), superoxide dismutase (SOD1), glutathione synthetase (GSS)  
264 and 5-oxoprolinase (OPLAH) (Figure 3A). IGF1 promotes the proliferation of Treg  
265 cells (Anguela et al., 2013). In SC patients, expression of IGF1 increased from the  
266 second to the sixth week, followed by a dramatic decrease in the seventh week, in line  
267 with the recovery of these patients (Figure 3A). However, in LC patients, expression  
268 of IGF1 slightly upregulated than in SC patients and increased until the eighth week,  
269 followed by a slow decline thereafter. The expression of IGF1 is higher in the LC  
270 patients than SC patients in the initial and the end of the disease stage (Figure 3A).  
271 Infection-induced ROS was reported to accelerate the accumulation of Treg cells,  
272 which led to immunosuppression (Yang et al., 2013). ROS may also induce the  
273 expression of SOD1 in the mitochondria to reduce ROS as negative feedback (Ma,  
274 2013). Our data showed that the expression of SOD1 peaked earlier in SC patients  
275 (fourth week) than that in the LC patients (fifth week, Figure 4A), indicating that  
276 clearance of infection-induced ROS in SC patients occurred earlier than in LC  
277 patients. GSS and OPLAH are both involved in the glutamyl cycle that maintains  
278 redox homeostasis (Forman et al., 2009). In the glutamyl cycle, GSS catalyzes the  
279 generation of reduced glutathione (GSH). OPLAH catalyzes the conversion of 5-  
280 oxoproline into glutamate and indirectly enhances the consumption of GSH. Our data  
281 showed that GSS was upregulated in the fourth week in SC patients, about one week  
282 earlier than its increase in LC patients (Figure 3A). In contrast, the downregulation of  
283 OPLAH began in the fourth week in SC patients, while in LC patients it did not  
284 substantially decrease until the eighth week (Figure 3A). The timely upregulation of  
285 GSS and downregulation of OPLAH might contribute to the elimination of infection-  
286 induced ROS in SC patients, while their delayed modulation may have contributed to  
287 the prolonged disease course of LC patients.

288

### 289 **Treg-mediated immunosuppression and crosstalk with other immune cells in the** 290 **LC patients**

291 The leukocyte migration and IGF/redox homeostasis pathway may modulate the  
292 activities of Th17 and Treg cells (Figure 3B). Th17 cells are a subset of T helper (Th)  
293 cells. Th17 cells are differentiated from CD4+ T cells with a pro-inflammatory role  
294 upon infection when IL6 is relatively high (Kimura and Kishimoto, 2010). The  
295 upregulation of IL-6 has been reported as one of the most critical cytokines in severe  
296 COVID-19 patients (Ruan et al., 2020). Our data suggested that activation of Th17  
297 cells may play a role in T cell immunity in COVID-19. Opposite to Th17 cells, Treg  
298 cells are induced from CD4+ T cells when IL-6 is relatively low and they suppress  
299 immunity (Kimura and Kishimoto, 2010).

300 Our data showed longitudinal down-regulation of DEFB1, an upstream activator  
301 of Th17. LC patients showed a delayed decrease of DEFB1, suggesting delayed

302 activation of Th17. IGF1 promotes Treg cells. A higher level of IGF1 in the LC  
303 patients suggested aberrant Treg-mediated immunosuppression in the LC patients  
304 (Figure 3A). Besides, infection-induced ROS, regulated by GSS and OPLAH, may  
305 also trigger Treg-mediated immunosuppression in LC patients as discussed above.

306 We next applied flow cytometry to analyze the CD127<sup>+</sup>CD25<sup>+</sup> Treg cell  
307 subpopulation in peripheral blood samples collected from disease onset to the fourth  
308 week (SC: 17 patients, 30 samples; LC: 17 patients, 22 samples). The data showed  
309 that the number of CD127<sup>+</sup>CD25<sup>+</sup> Treg cells was significantly higher in LC patients  
310 than that in SC patients ( $p=0.006$ ), while the CD45<sup>+</sup> lymphocytes ( $p=0.306$ ) and  
311 CD3<sup>+</sup>CD4<sup>+</sup> T cells ( $p=0.871$ ) did not show a significant difference (Figure 4A). The  
312 data support the hypothesis that CD127<sup>+</sup>CD25<sup>+</sup> Treg-mediated immunosuppression  
313 may be induced in LC patients during the first few weeks. Inhibition of Treg cells  
314 could be a potential therapeutic approach for COVID-19 patients with long disease  
315 course.

316 More natural killer (NK) cells, especially the cytotoxic subset (CD3<sup>-</sup>  
317 CD56<sup>+</sup>CD16<sup>+</sup>), were found in LC patients (Figure 4B). NK cells are a typical kind of  
318 cells in innate immunity. In the meantime, CD3<sup>-</sup>CD56<sup>-</sup>CD16<sup>-</sup> cells were found to be  
319 decreased in the LC group (Figure S6A-B). These cells are probably B cells, which is  
320 further supported by our finding that the antibody level of these patients were also  
321 decreased (Huang, 2020). The decrease of B cells may also be supported by the  
322 finding that NK cells can inhibit the B cell immunity through reducing neutralizing  
323 antibodies (Rydyznski et al., 2015). However, unfortunately we did not have sufficient  
324 sample to stain these reduced cells with markers for B cells to confirm their identity.

325 We then measured the key cytokines and growth factors such as IL-2, IL-4, IL-5,  
326 IL-6, IL-10, IL-17A, IFN- $\gamma$ , and TNF- $\alpha$  of clinical importance. They were measured  
327 using antibody-based method (SC: 17 patients, 30 samples; LC: 17 patients, 22  
328 samples; Figure 5B and Figure S6C). Except for TNF- $\alpha$ , other molecules showed no  
329 difference between SC and LC patients, probably because most patients in this study  
330 were non-severe cases (Figure 5B). TNF- $\alpha$  was found to be increases in the LC group,  
331 which might be associated with the upregulated NK cells.

332 However, in our proteomics data, we identified two key receptors for IL-6,  
333 namely the alpha subunit (IL6R) and the beta subunit (IL6ST) of the interleukin-6  
334 receptor. These two subunits are jointly required to mediate IL-6 signal transmission.  
335 Overall, LC patients expressed higher IL6ST than SC patients did (Figure 5).  
336 Interestingly, IL6R was upregulated in LC patients during the first four weeks  
337 followed by a decline thereafter. In SC patients, IL6R expression did not show the  
338 substantial change (Figure 5). This difference of IL6R expression trends may reflect  
339 transient activation of Th17 during the prolonged disease course. We also detected the  
340 dynamics of two proteins, transforming growth factor beta-1 protein (TGFB1) and  
341 cytosol aminopeptidase (LAP3), which are associated with Treg function. LAP3 is  
342 one of the surface markers of Treg, and TGFB1 regulated Treg and Th17 (Oida et al.,  
343 2003). Similar to IL6ST, LAP3 also kept a higher level in the LC group across the  
344 disease course than in SC patients (Figure 5). TGFB1 showed no difference between  
345 the SC and LC patients (Figure 5).



346 Taken together, our data showed that NK cell-mediated innate immune and Treg-  
347 mediated immunosuppression were both activated in the LC group, while CD3<sup>+</sup>CD56<sup>-</sup>  
348 CD16<sup>-</sup> cells were decreased in the LC group, suggesting suppression of B cells which  
349 may be associated with decreased antibody level.

350

### 351 **Predictive model for the length of disease course**

352 The above analysis showed that SC and LC patients have different proteomic  
353 serological responses during the early phase of COVID-19 when the two groups of  
354 patients were clinically indistinguishable during the first few weeks (Figure S1). This  
355 raises the possibility of predicting disease course based on proteomic patterns during  
356 the early phase. To test this, we built a random forest model using the serum  
357 proteomic data collected during the first three weeks. We included a total of 80 serum  
358 samples as a discovery dataset (Figure 6A) which were randomly divided into two  
359 groups: a 66-sample training dataset (30 patients and 66 samples) and a validation  
360 dataset (7 patients and 14 samples). Next, a previously published cohort (39 patients  
361 and 39 samples) (Shen, 2020) was employed as an independent test dataset from a  
362 different clinical center.

363 To select the most relevant proteins (referred as “feature” in machine learning),  
364 we retrieved 174 significantly differentially expressed proteins from the proteomic  
365 profiling of SC and LC patients during the first three weeks (Table S3). These proteins  
366 were also identified in the independent test dataset. Then 58 features with highest  
367 predictive accuracy were prioritized from the training set using random forest (4.6.14)  
368 (Figure 6A, Figure S7A). After a six-fold cross-validation between the training set and  
369 the validation set, a classifier with 35 feature proteins was finalized for classifying LC  
370 patients with 100% accuracy in the training set (Figure 6A). The details of the 35 key  
371 features are shown in Figure 6B. Intercellular adhesion molecule 1 (ICAM1), low  
372 affinity immunoglobulin gamma Fc region receptor 3-A (FCGR3A) and  
373 immunoglobulin kappa variable 1-16 (IGKV1-16) are the top three ranked proteins,  
374 which were significantly regulated in LC patients within the first three weeks (Figure  
375 S7B). ICAM1 mediates cell-cell contact and promotes T cell apoptosis (Starke et al.,  
376 2010). FCGR3A is involved in antibody-dependent cell-mediated cytotoxicity  
377 (ADCC). The elevation of FCGR3A is consistent with the increase of NK cells in the  
378 LC group. IGKV1-16 is a part of the variable domain of immunoglobulin light chain,  
379 and it is secreted by B cell. IGKV1-16 was down-regulated in the LC group, which  
380 might be associated with dysregulation of B cell in the LC as discussed previously.

381 We then applied the model to the independent test cohort from a different clinical  
382 center. The model correctly classified 32 out of 39 patients with an overall accuracy of  
383 82% (Figure 6C). Due to biosafety issues and the emergency of this pandemic, this  
384 study is limited by the sample size. We noticed that the distribution of samples in the  
385 different disease stage is different between discovery dataset and test dataset. The  
386 numbers of serum samples of the discovery dataset are 18, 31 and 31 for the first,  
387 second and the third week, respectively. However, the numbers for the test dataset are  
388 21, 14 and 4, showing substantially lower proportions in the second and third week.  
389 This difference was significant as measured by a two-sides Fisher’s exact test ( $p =$

390 0.0004). The substantially higher number of samples collected in the first week have  
391 probably contributed to the difficulty of correct classification by this model. Indeed,  
392 the prediction accuracy was 92.9% for the samples collected in the second and third  
393 weeks, while the accuracy was only 72.2% for the samples collected in the first week.  
394 Future application and improvement of this model in larger clinical cohorts are  
395 needed.

## 396 **Conclusion**

397 COVID-19 patients with short and long disease courses showed no significant  
398 difference in clinical symptoms, laboratory tests and response to conventional therapy.  
399 Our longitudinal sera proteomic analysis uncovered characteristic host responses in  
400 sera of patients with long disease course, including enhanced NK cell-mediated innate  
401 immune response and Treg-mediated immunosuppression at an early stage. Our data  
402 also suggested CD3<sup>+</sup>CD56<sup>-</sup>CD16<sup>-</sup> cells might contribute to decreased production of S  
403 protein specific antibodies in the patients with a prolonged disease course. Our data  
404 suggest modulation of Treg cells may be potential therapeutics for these COVID-19  
405 patients. We also showed that it is possible to predict the disease course of COVID-19  
406 patients based on selected protein levels within the first three weeks after disease  
407 onset. The model nevertheless requires further validation in independent cohorts.  
408

## 409 **ACKNOWLEDGMENTS**

410 This work is supported by grants from Tencent Foundation (2020), National Natural  
411 Science Foundation of China (81972492, 21904107, 81672086), Zhejiang Provincial  
412 Natural Science Foundation for Distinguished Young Scholars (LR19C050001), and  
413 Hangzhou Agriculture and Society Advancement Program (20190101A04). We thank  
414 Drs O.L. Kon, H. Qi, H. Xu, and X. Chang for helpful comments to this study, and  
415 Westlake University Supercomputer Center and biomedical research core facilities for  
416 assistance in data generation and analysis.  
417

## 418 **AUTHOR CONTRIBUTIONS**

419 T.G., S.T., Y.Z. and J.H. designed and supervised the project. S.T., J.H., T.M., C.  
420 H., S.L., X.X., H.L., L.W., J.D. collected the samples and clinical data. R.S., Q.X.,  
421 W.G., M.L., L.Q., H.C., Q.Z., S.L., W.L., H.G., L.L., T.L., X.L., X.C., and G.R.  
422 conducted proteomic analysis. T.M., Q.X. and R.S. performed flow cytometry  
423 analysis. R.S., Q.X., W.G., T.M., C.H., Y.Z., S.T. and T.G. interpreted the data with  
424 inputs from all co-authors. R.S., Q.X., Y.Z. and T.G. wrote the manuscript with  
425 inputs from co-authors.  
426

## 427 **DECLARATION OF INTERESTS**

428 This study is partly supported by Tecent.  
429

## 430 REFERENCES

- 431 Anguela, X.M., Tafuro, S., Roca, C., Callejas, D., Agudo, J., Obach, M., Ribera, A., Ruzo, A., Mann,  
432 C.J., Casellas, A., *et al.* (2013). Nonviral-mediated hepatic expression of IGF-I increases Treg levels  
433 and suppresses autoimmune diabetes in mice. *Diabetes* *62*, 551-560.
- 434 Brown, J.A., Dorfman, D.M., Ma, F.R., Sullivan, E.L., Munoz, O., Wood, C.R., Greenfield, E.A., and  
435 Freeman, G.J. (2003). Blockade of programmed death-1 ligands on dendritic cells enhances T cell  
436 activation and cytokine production. *J Immunol* *170*, 1257-1266.
- 437 Cao, X. (2020). COVID-19: immunopathology and its implications for therapy. *Nat Rev Immunol* *20*,  
438 269-270.
- 439 Colaert, N., Barsnes, H., Vaudel, M., Helsens, K., Timmerman, E., Sickmann, A., Gevaert, K., and  
440 Martens, L. (2011). Thermo-msf-parser: an open source Java library to parse and visualize Thermo  
441 Proteome Discoverer msf files. *J Proteome Res* *10*, 3840-3843.
- 442 di Comite, G., Marinosci, A., Di Matteo, P., Manfredi, A., Rovere-Querini, P., Baldissera, E., Aiello, P.,  
443 Corti, A., and Sabbadini, M.G. (2006). Neuroendocrine modulation induced by selective blockade of  
444 TNF-alpha in rheumatoid arthritis. *Ann N Y Acad Sci* *1069*, 428-437.
- 445 Eissa, N., Hussein, H., Kermarrec, L., Ali, A.Y., Marshall, A., Metz-Boutigue, M.H., Hendy, G.N.,  
446 Bernstein, C.N., and Ghia, J.E. (2018). Chromogranin-A Regulates Macrophage Function and the  
447 Apoptotic Pathway in Murine DSS colitis. *J Mol Med (Berl)* *96*, 183-198.
- 448 Forman, H.J., Zhang, H., and Rinna, A. (2009). Glutathione: overview of its protective roles,  
449 measurement, and biosynthesis. *Mol Aspects Med* *30*, 1-12.
- 450 Gao, H., Zhang, F., Liang, S., Zhang, Q., Lyu, M., Qian, L., Liu, W., Ge, W., Chen, C., Yi, X., *et al.*  
451 (2020). Accelerated Lysis and Proteolytic Digestion of Biopsy-Level Fresh-Frozen and FFPE Tissue  
452 Samples Using Pressure Cycling Technology. *J Proteome Res* *19*, 1982-1990.
- 453 Goncalves, C.M., Castro, M.A., Henriques, T., Oliveira, M.I., Pinheiro, H.C., Oliveira, C., Sreenu,  
454 V.B., Evans, E.J., Davis, S.J., Moreira, A., *et al.* (2009). Molecular cloning and analysis of SSc5D, a  
455 new member of the scavenger receptor cysteine-rich superfamily. *Mol Immunol* *46*, 2585-2596.
- 456 Hu, J., Yan, J., Rao, G., Latha, K., Overwijk, W.W., Heimberger, A.B., and Li, S. (2016). The Duality  
457 of Fgl2 - Secreted Immune Checkpoint Regulator Versus Membrane-Associated Procoagulant:  
458 Therapeutic Potential and Implications. *Int Rev Immunol* *35*, 325-339.
- 459 Huang, J.e.a. (2020). Long period dynamics of viral load and antibodies for SARS-CoV-2 infection: an  
460 observational cohort study. medRxiv <https://doi.org/10.1101/2020.04.22.20071258>.
- 461 Ivetic, A., Deka, J., Ridley, A., and Ager, A. (2002). The cytoplasmic tail of L-selectin interacts with  
462 members of the Ezrin-Radixin-Moesin (ERM) family of proteins: cell activation-dependent binding of  
463 Moesin but not Ezrin. *J Biol Chem* *277*, 2321-2329.
- 464 Kemper, C., Chan, A.C., Green, J.M., Brett, K.A., Murphy, K.M., and Atkinson, J.P. (2003). Activation  
465 of human CD4+ cells with CD3 and CD46 induces a T-regulatory cell 1 phenotype. *Nature* *421*, 388-  
466 392.
- 467 Kimura, A., and Kishimoto, T. (2010). IL-6: regulator of Treg/Th17 balance. *Eur J Immunol* *40*, 1830-  
468 1835.
- 469 Kumar, L., and Mattias, E.F. (2007). Mfuzz: a software package for soft clustering of microarray data.  
470 *Bioinformatics* *2*, 5-7.
- 471 Li, J., Van Vranken, J.G., Pontano Vaites, L., Schweppe, D.K., Huttlin, E.L., Etienne, C., Nandhikonda,  
472 P., Viner, R., Robitaille, A.M., Thompson, A.H., *et al.* (2020). TMTpro reagents: a set of isobaric

473 labeling mass tags enables simultaneous proteome-wide measurements across 16 samples. *Nat*  
474 *Methods* *17*, 399-404.

475 Messner, e.a. (2020). Ultra-high-throughput clinical proteomics reveals classifiers of COVID-19  
476 infection. *Cell Systems*, <https://doi.org/10.1016/j.cels.2020.1005.1012>.

477 Oida, T., Zhang, X., Goto, M., Hachimura, S., Totsuka, M., Kaminogawa, S., and Weiner, H.L. (2003).  
478 CD4+CD25- T cells that express latency-associated peptide on the surface suppress  
479 CD4+CD45RBhigh-induced colitis by a TGF-beta-dependent mechanism. *J Immunol* *170*, 2516-2522.

480 Ruan, Q., Yang, K., Wang, W., Jiang, L., and Song, J. (2020). Clinical predictors of mortality due to  
481 COVID-19 based on an analysis of data of 150 patients from Wuhan, China. *Intensive Care Med* *46*,  
482 846-848.

483 Shen, B., *et al.* (2020). Proteomic and Metabolomic Characterization of COVID-19 Patient Sera.  
484 medRxiv.

485 Starke, A., Lindenmeyer, M.T., Segerer, S., Neusser, M.A., Rusi, B., Schmid, D.M., Cohen, C.D.,  
486 Wuthrich, R.P., Fehr, T., and Waeckerle-Men, Y. (2010). Renal tubular PD-L1 (CD274) suppresses  
487 alloreactive human T-cell responses. *Kidney Int* *78*, 38-47.

488 Thompson, A., Wolmer, N., Koncarevic, S., Selzer, S., Bohm, G., Legner, H., Schmid, P., Kienle, S.,  
489 Penning, P., Hohle, C., *et al.* (2019). TMTpro: Design, Synthesis, and Initial Evaluation of a Proline-  
490 Based Isobaric 16-Plex Tandem Mass Tag Reagent Set. *Anal Chem* *91*, 15941-15950.

491 To, K.K., Tsang, O.T., Leung, W.S., Tam, A.R., Wu, T.C., Lung, D.C., Yip, C.C., Cai, J.P., Chan, J.M.,  
492 Chik, T.S., *et al.* (2020). Temporal profiles of viral load in posterior oropharyngeal saliva samples and  
493 serum antibody responses during infection by SARS-CoV-2: an observational cohort study. *Lancet*  
494 *Infect Dis*.

495 Ueda, Y., Katagiri, K., Tomiyama, T., Yasuda, K., Habiro, K., Katakai, T., Ikehara, S., Matsumoto, M.,  
496 and Kinashi, T. (2012). Mst1 regulates integrin-dependent thymocyte trafficking and antigen  
497 recognition in the thymus. *Nat Commun* *3*, 1098.

498 Wojtowicz, A., Gresnigt, M.S., Lecompte, T., Bibert, S., Manuel, O., Joosten, L.A., Rueger, S., Berger,  
499 C., Boggian, K., Cusini, A., *et al.* (2015). IL1B and DEFB1 Polymorphisms Increase Susceptibility to  
500 Invasive Mold Infection After Solid-Organ Transplantation. *J Infect Dis* *211*, 1646-1657.

501 Wu, D., Shu, T., Yang, X., Song, J.-X., Zhang, M., Yao, C., Liu, W., Huang, M., Yu, Y., Yang, Q., *et al.*  
502 (2020). Plasma Metabolomic and Lipidomic Alterations Associated with COVID-19. *National Science*  
503 *Review*.

504 Wu, Z., and McGoogan, J.M. (2020). Characteristics of and Important Lessons From the Coronavirus  
505 Disease 2019 (COVID-19) Outbreak in China: Summary of a Report of 72314 Cases From the Chinese  
506 Center for Disease Control and Prevention. *JAMA*.

507 Yang, D., Rosenberg, H.F., Chen, Q., Dyer, K.D., Kurosaka, K., and Oppenheim, J.J. (2003).  
508 Eosinophil-derived neurotoxin (EDN), an antimicrobial protein with chemotactic activities for dendritic  
509 cells. *Blood* *102*, 3396-3403.

510 Yang, X., Yu, Y., Xu, J., Shu, H., Xia, J., Liu, H., Wu, Y., Zhang, L., Yu, Z., Fang, M., *et al.* (2020).  
511 Clinical course and outcomes of critically ill patients with SARS-CoV-2 pneumonia in Wuhan, China:  
512 a single-centered, retrospective, observational study. *Lancet Respir Med*.

513 Yang, Y., Bazhin, A.V., Werner, J., and Karakhanova, S. (2013). Reactive oxygen species in the  
514 immune system. *Int Rev Immunol* *32*, 249-270.

515 Zhou, F., Yu, T., Du, R., Fan, G., Liu, Y., Liu, Z., Xiang, J., Wang, Y., Song, B., Gu, X., *et al.* (2020).  
516 Clinical course and risk factors for mortality of adult inpatients with COVID-19 in Wuhan, China: a

517 retrospective cohort study. *Lancet* 395, 1054-1062.  
518 Zhou, Y., Zhou, B., Pache, L., Chang, M., Khodabakhshi, A.H., Tanaseichuk, O., Benner, C., and  
519 Chanda, S.K. (2019). Metascape provides a biologist-oriented resource for the analysis of systems-  
520 level datasets. *Nat Commun* 10, 1523.  
521  
522



523 **Table 1. Baseline and progression of CVDTSA cohort**

Baseline Characteristic	non-COVID-19 (N=35)	COVID-19 SC (N=17)	COVID-19 LC (N=20)
<b>Gender — no. <sup>a</sup>(%)</b>			
male	17 (53.1)	8 (47.1)	11 (55.0)
female	15 (47.9)	9 (52.9)	9 (45.0)
<b>Age — yr <sup>b</sup></b>			
mean ± SD	43.0 ± 18.0	43.2 ± 10.5	49.0 ± 15.4
median (IQR)	37.5 (28.8-56.0)	44 (35.0-50.0)	50 (42.8-55.5)
range	18-80	27-67	2-84
<b>Symptoms —no. (%)</b>			
fever	28 (87.6)	10 (58.8)	14 (70.0)
cough	2 (6.3)	11 (64.7)	15 (75.0)
diarrhea	1 (3.1)	10 (58.8)	8 (40.0)
fatigue	1 (3.1)	8 (47.1)	7 (35.0)
<b>Comorbidities — no. (%)</b>			
hypertension		2 (11.8)	6 (30.0)
diabetes		0 (0.0)	3 (15.0)
hepatitis B		2 (11.8)	0 (0.0)
coronary sclerosis		0 (0.0)	3 (15.0)
gastrohelcosis		1 (5.9)	0 (0.0)
psoatic strain		0 (0.0)	1 (5.0)
chronic gynecologic inflammation		1 (5.9)	0 (0.0)
gout		0 (0.0)	1 (5.0)
asthma		0 (0.0)	1 (5.0)
<b>Treatment— no. (%)</b>			
lopinavir and ritonavir		17 (100.0)	19 (95.0)
Atomized interferon		17 (100.0)	20 (100.0)
Arbidol		7 (41.2)	12 (60.0)
Lianhuaqingwen (Chinese traditional medicine)		15 (88.2)	16 (80.0)
Ribavirin		0 (0.0)	3 (15.0)
Hydroxychloroquine		1 (5.9)	3 (15.0)

<sup>a</sup> no.: number.

<sup>b</sup> yr.: year

524

525

## 526 **Figure legend**

527 **Figure 1. Patients, samples and study workflow.** (A) Baseline characteristics of the  
528 study cohort. The y-axis shows the patient ID, and the x-axis displays the length of  
529 disease course from onset. The 37 patients are separated into SC (17 patients) and LC  
530 (20 patients) groups. Other important information including the virus nucleic acid test  
531 results (sputum/throat swab-positive/-negative), gender, severity, comorbidity  
532 baseline, etc., are shown in the right panel of the figure. The black dots indicate  
533 sampling time. More details are provided in Table S1. (B) Workflow for TMT based  
534 proteomic analysis in this study. 37 COVID-19 patients and 32 control (Ctrl) patients  
535 were included. In total, 224 sera samples were collected and 268 peptide samples  
536 including 44 technical replicates were analyzed by TMT 16plex-based quantitative  
537 proteomics.

538 **Figure 2. Complex immunity in the LC patients.** (A) Summary of enriched  
539 immune-related pathways in LC and SC patients across the disease course.  
540 Representative proteins involved in these pathways are also shown. (B) Venn diagram  
541 of differentially expressed proteins between the SC and LC groups over nine time  
542 points and specifically regulated in COVID-19 sera. (C) Heatmap of 97 dysregulated  
543 proteins in the SC and LC groups over nine time points. (D-E) Expression of protein  
544 group 1 and 2 across nine time points. The y-axis stands for the relative protein  
545 expression normalized by z-score. The pathways and representative participating  
546 proteins are shown below the boxplots.

547 **Figure 3. Characteristic proteins and pathways in LC patients.** (A) Representative  
548 proteins involved in leukocyte migration and IGF/redox homeostasis are plotted over  
549 time. (B) Diagram depicting that major regulated pathways in the LC patients  
550 including leukocytes migration and IGF/redox homeostasis jointly modulate Treg-  
551 mediated immunosuppression.

552 **Figure 4. Flow cytometric analysis of immune cells between SC and LC patients.**  
553 22 samples from 17 LC patients and 30 samples from 17 SC patients were analyzed.  
554 (A) Flow cytometric analysis of lymphocytes, CD4<sup>+</sup> cells and CD127-CD25<sup>+</sup> Treg  
555 cells of two representative patients. Bean plots show the comparison between the two  
556 groups. (B) Flow cytometric analysis of lymphocytes, CD8<sup>+</sup> cells and CD56<sup>+</sup>CD16<sup>+</sup>  
557 NK cells of two representative patients. Bean plots show the comparison between the  
558 two groups.

559 **Figure 5. Dynamics of IL6ST, IL6R, LAP3 and TGFB1 in SC and LC patients.**  
560 (A) Proteins detected by MS-based proteomics. (B) Violin plot showed that cytokines  
561 detected by antibody-based flow cytometric analysis (24 samples from 13 SC patients  
562 and 19 samples from 12 LC patients).

563 **Figure 6. Machine learning model for predicting disease course.** (A) Workflow for  
564 machine learning. (B) The top 35 key feature proteins selected by the machine  
565 learning model. (C) The validation of the model in an independent test dataset.

566 **METHODS**

567 **KEY RESOURCES TABLE**

<b>REAGENT or RESOURCE</b>	<b>SOURCE</b>	<b>IDENTIFIER</b>
<b>Biological Samples</b>		
<b>Serum samples from 37 COVID-19 patients and 34 non-COVID-19 patients</b>	Wenzhou Central Hospital	This paper
<b>Chemicals, Peptides, and Recombinant Proteins</b>		
<b>Triethylammonium bicarbonate buffer (TEAB)</b>	Sigma-Aldrich	Cat # T7408
<b>Pierce™ Micro-spin column</b>	Thermo Fisher Scientific	Cat # 89868
<b>High Select™ Top14 abundant protein depletion resin</b>	Thermo Fisher Scientific	Cat # A36372
<b>3K MWCO pierce protein concentrators</b>	Thermo Fisher Scientific	Cat # 88521
<b>Urea</b>	Sigma-Aldrich	Cat # U1250
<b>Tris (2-carboxyethyl) phosphine (TCEP)</b>	Adamas-beta	Cat # 61820E
<b>Iodoacetamide (IAA)</b>	Sigma-Aldrich	Cat # I6125
<b>Trypsin</b>	Hualishi Tech	Cat # HLS TRY001C
<b>Trifluoroacetic acid (TFA)</b>	Thermo Fisher Scientific	Cat # 85183
<b>Water</b>	Thermo Fisher Scientific	Cat # W6-4
<b>Acetonitrile</b>	Thermo Fisher Scientific	Cat # A955-4
<b>Formic acid (FA)</b>	Thermo Fisher Scientific	Cat # A117-50
<b>Ammonium hydroxide solution</b>	Sigma-Aldrich	Cat # 221228
<b>Methanol</b>	Sigma-Aldrich	Cat # 34860
<b>Critical Commercial Assays</b>		
<b>TMTpro™ 16plex reagents</b>	Thermo Fisher Scientific	Cat # A44520
<b>SARS-CoV-2 nucleic acid detection kit</b>	Shanghai BioGerm Medical Technology	Cat # 20200125E
<b>CD4-PE-Cy7</b>	UB Biotechnology	Cat # UB105441
<b>CD3-FITC</b>	UB Biotechnology	Cat # UB104411
<b>CD25-PE</b>	UB Biotechnology	Cat # UB112421
<b>CD45-PerCP-Cy5.5</b>	UB Biotechnology	Cat # UB109481
<b>CD127-APC</b>	UB Biotechnology	Cat # UB113451
<b>CD8-PE</b>	UB Biotechnology	Cat # UB106421
<b>CD16-PE-Cyanine7</b>	UB Biotechnology	Cat # UB107441
<b>CD56-PE</b>	UB Biotechnology	Cat # UB108421
<b>Cytokines detection kit including IL-2/IL-4/IL-5/IL-6/IL-10/IL-17A/TNF-<math>\alpha</math>/IFN-<math>\gamma</math></b>	UB Biotechnology	Cat # UB06PX

<b>Software and Algorithms</b>				
<b>Xcalibur</b>			Thermo Fisher Scientific	Cat # OPTON-30965
<b>Proteome Discoverer 2.4.1.15</b>		<b>Version</b>	Thermo Fisher Scientific	<a href="https://www.thermo-fisher.com/hk/en/home/industrial/mass-spectrometry/liquid-chromatography-mass-spectrometry-lc-ms/lc-ms-software/multi-omics-data-analysis/proteome-discoverer-software.html">https://www.thermo-fisher.com/hk/en/home/industrial/mass-spectrometry/liquid-chromatography-mass-spectrometry-lc-ms/lc-ms-software/multi-omics-data-analysis/proteome-discoverer-software.html</a>
<b>R version 3.6.1</b>			R Project	<a href="https://www.r-project.org">https://www.r-project.org</a>
<b>Ingenuine pathway analysis (version 51963813)</b>			Kramer et al., 2014	<a href="https://www.qiagen.com/cn/">https://www.qiagen.com/cn/</a>
<b>Kaluza analysis soft version 2.1</b>			Beckman coulter life sciences	Cat # A82959
<b>NovoExpress version 1.4.1</b>			Agilent Bio	<a href="https://www.aceabio.com/products/novoexpress-software/">https://www.aceabio.com/products/novoexpress-software/</a>
<b>Other</b>				
<b>SOLA<math>\mu</math></b>			Thermo Fisher Scientific	Cat # 62209-001
<b>ACQUITY UPLC Systems with 2D LC Technology</b>			Waters Corporation	Cat # 186015001
<b>ACQUITY BEH C18 column, 2.1 × 100 mm, 1.7 <math>\mu</math>m</b>			Waters Corporation	Cat # 186008316
<b>ACQUITY BEH Amide column, 2.1 × 100 mm, 1.7 <math>\mu</math>m</b>			Waters Corporation	Cat # 186008315

568

## 569 **RESOURCE AVAILABILITY**

### 570 **Lead contact**

571 Further information should be directed to and will be fulfilled by the Lead Contact  
572 Tiannan Guo ([guotiannan@westlake.edu.cn](mailto:guotiannan@westlake.edu.cn)).

573

### 574 **Materials Availability**

575 This study did not generate new unique reagents.

576

### 577 **Data Availability**

578 All data are available in the manuscript or the supplementary materials. The  
579 proteomics data are deposited in ProteomeXchange Consortium  
580 (<https://www.iprox.org/>). Project ID: IPX0002170000. All the data will be publicly  
581 released upon publication.

582

## 583 **EXPERIMENTAL MODEL AND SUBJECT DETAILS**

### 584 **Patients and sera samples**

585 We procured 72 patients in this study, including 37 COVID-19 patients whose  
586 sputa or throat swabs were tested positive for SARS-CoV-2 according to the  
587 manufacturer's instructions (Shanghai BioGerm Medical Technology Co., LTD,  
588 Shanghai, China). According to the Chinese Government Diagnosis and Treatment  
589 Guideline (Trial 4th version) (Shen, 2020), these 37 COVID-19 patients include 35  
590 typical cases and two severe cases. We have also procured 35 non-COVID-19  
591 patients showing similar flu-like clinical symptoms to COVID-19 patients with  
592 negative nucleic acid testing for SARS-CoV-2. More details of these patients are  
593 provided in Figure 1A and Table S1.

594 We defined the disease onset as the day when the patient manifests clinical  
595 symptoms, while the disease recovery as the day when nucleic acid test of sputa or  
596 throat swab turns negative, and negative for the second test after a minimal interval of  
597 24 hours, the same test is still negative. The disease course was thus defined as the  
598 period between disease onset and disease recovery.

599 Totally 224 sera samples from these patients were collected longitudinally for  
600 proteomics analysis (Figure 1B, Table S1). Sampling was performed in the early  
601 morning before diet using serum separation tubes (BD, USA). The blood was  
602 clotted for about 30 min at room temperature, and then centrifuged at 1000 g for ten  
603 min for serum sample collection. This study has been registered in the Chinese  
604 Clinical Trial Registry with an ID of ChiCTR2000031699. This study has been  
605 approved by the Ethical/Institutional Review Board of Wenzhou Central Hospital and  
606 Westlake University. Contents from patients were waived by the boards.

607

## 608 **METHOD DETAILS**

609



## 610 **Proteome analysis**

611 Serum samples were prepared as previously described (Shen, 2020). Briefly, serum  
612 samples were firstly inactivated and sterilized at 56 °C for 30 mins. For proteomic  
613 study, 4 µL of serum was used for each sample. The serum was firstly depleted of  
614 14 high abundant serum proteins using a human affinity depletion kit (Thermo  
615 Fisher Scientific™, San Jose, USA). After depletion, the serum solution was  
616 concentrated into 50 µL through a 3k MWCO filtering unit (Thermo Fisher  
617 Scientific™, San Jose, USA) according to manufacturer. And then was mixed with  
618 500 µL 8 M urea (Sigma) and concentrated into 50 µL. Then proteins were reduced  
619 and alkylated with 10 mM tris (2-carboxyethyl) phosphine (TCEP, Sigma) and 40  
620 mM iodoacetamide (IAA), respectively. Proteins were submitted to two times of  
621 tryptic digestion (enzyme to protein ratio: 1:20; Hualishi Tech. Ltd, Beijing, China).  
622 The digestion was then stopped with 1% trifluoroacetic (TFA) (Thermo Fisher) to  
623 pH 2–3 to stop the reaction, and peptides were subjected to C18 (Thermo Fisher)  
624 desalting.

625 TMT 16-plex (Thermo Fisher) reagents were applied to label the digested  
626 peptides. The TMT labeled samples were further fractionated along a 2 hr basic pH  
627 reverse phase LC gradient using a Dinex Ultimate 3000 UHPLC (Thermo Fisher)  
628 (Li et al., 2020). LC-MS/MS analysis was performed using the Easy-nLC™ 1200  
629 nanoLC-MS/MS system (Thermo Fisher) or a Dinex Ultimate 3000 UHPLC  
630 coupled to a Q Exactive HF or HF-X (Thermo Fisher), along a 60 min LC gradient  
631 at a flowrate of 300 nL/min as described previously (Gao et al., 2020; Shen, 2020).  
632 To reach comparable proteomic depth, the fractionated samples were combined into  
633 30 fractions for analysis in QE-HF instruments and 26 for QE-HFX instruments.

634

## 635 **Database search and statistical analysis**

636 MS data was performed using Proteome Discoverer (Version 2.4.1.15, Thermo  
637 Fisher) (Colaert et al., 2011) search engine against the human protein  
638 database downloaded from UniProt (version 02/01/2020; 164,930 sequences), with a  
639 precursor ion mass tolerance of 10 ppm and fragment ion mass tolerance of 0.02 Da.  
640 Please see previous paper (Shen, 2020) for detailed parameters of the database  
641 searching. Briefly, TMT pro-plex labels to lysine and N-terminus, and  
642 carbamidomethylation of cysteine were set as static modifications. A cut-off  
643 criterion of a q-value of 0.01, corresponding to a 1% false-discovery rate (FDR) was  
644 set for the filtered of identified peptides with highly confident peptide hits.

645 After filtering 80% missing rate proteins, 2700 proteins used for differential  
646 expression analysis based on  $|\log_2(\text{FC})|$  and two-sided unpaired Welch's t test. The  
647 created missing values were imputed with zero.

648

## 649 **Pathway analysis**

650 For the pathway enrichment analysis, firstly, four databases including KEGG  
651 pathway, GO biological processes, Reactome gene sets and immunologic signatures  
652 were used for immune characterization analysis on the Metascape web-based

653 platform (Zhou et al., 2019). IPA was then used to look at the pathways for  
654 differentially expressed proteins.

655

### 656 **Statistical analysis**

657 Two-sided unpaired Welch's t test was performed for each pair of comparing  
658 groups. The one-way analysis of variance (ANOVA) was used to performed among  
659 nine time points. Adjusted p values were calculated using Benjamini & Hochberg  
660 correction.

661

### 662 **Machine learning**

663 The machine learning was performed using the R package randomForest (version  
664 4.6.14) as described previously with some modifications (Shen, 2020) as described  
665 briefly in the following. The discovery dataset was divided into two parts, *i.e.* the  
666 training set and the validation set. We optimized the key random forest parameters  
667 including the cutoff values for decrease mean accuracy, cross-validation fold, and the  
668 number of trees. Input protein features were selected based on the mean decrease  
669 accuracy cutoff. For the optimized model, the minimal mean decrease accuracy of  
670 protein features was 2, the mtry was set as 13, and 800 trees were built. Six-fold cross  
671 validation was performed and this was repeated 100 times.

672

### 673 **Flow cytometry analysis**

674 Peripheral blood samples from EDTA anticoagulants were incubated with  
675 mixture antibodies including CD4-PE-Cy7 (UB105441, UB Biotechnology Co., Ltd,  
676 Hangzhou, China), CD3-FITC (UB104411), CD25-PE (UB112421), CD45-PerCP-  
677 Cy5.5 (UB109481), CD127-APC (UB113451) and a kit (UB06PX) for cytokines  
678 detection including IL-2/IL-4/IL-5/IL-6/IL-10/IL-17A/TNF- $\alpha$ /IFN- $\gamma$  for 15 min at  
679 room temperature. Double negative control and single-stain controls were prepared by  
680 normal samples, and were used to calculate a compensation matrix. Sample  
681 acquisition was performed on a Gallios (Beckman Coulter) cytometer equipped. Final  
682 analysis and graphical output were performed using NovoExpress software (Agilent  
683 Bio).

684

## 685 SUPPLEMENTARY FIGURE LEGEND

686 **Figure S1. Correlation analysis between the SC and LC group based on clinical**  
687 **data, Related to Figure 1. (A)** Boxplot of patient ages. Ctrl (N=35), SC (N=17) and  
688 LC(N=20). **(B)** Heatmap shows medication history in SC and LC groups. The column  
689 set on the right represents the drugs and relevant p value showing medication  
690 difference between the two groups (two-sided Fisher. test). **(C)** Comparison of blood  
691 test results between SC (N=17) and LC (N=15) patients. Boxplots display the blood  
692 biochemistry tests based on samples collected on the first day in the hospital.

693 **Figure S2. Quality assessment of proteomics data. Related to Figure 1. (A)** Batch  
694 design of proteomic analysis. All 268 peptide samples are randomly separated into 18  
695 batches for TMTpro labeling and MS analysis. **(B)** The median technical CV of the  
696 proteomics data is calculated by the identified proteins in 44 technical replicates.

697 **Figure S3. Pathway enrichment analysis at nine time points using differentially**  
698 **expressed proteins between the SC and LC group, Related to Figure 2.** Pathways  
699 were enriched using Metascape. The pathways in the blue box are not directly  
700 related to immunity.

701 **Figure S4. The dynamic expression of proteins across the entire disease course**  
702 **between SC and LC, Related to Figure 2.** The x-axis shows the week index, while  
703 the y-axis denotes protein expression ratio from the TMT experiment. Pair-wise  
704 comparison of each proteins in the two patient groups was performed with student's *t*  
705 test. \*,  $p < 0.05$ ; \*\*,  $p < 0.01$ .

706 **Figure S5. Eight clusters of proteins showing temporal dynamics by Mfuzz**  
707 **analysis in the SC and LC group, Related to Figure 4.** Proteins detected in SC **(A)**  
708 and LC **(B)** are grouped into eight clusters with different quantitative patterns over the  
709 disease course. ANOVA analysis was performed in each cluster (the cutoff of the  
710 adjusted p value (BH adjust) was 0.05). **(C)** Upset plots shows the overlapping protein  
711 clusters selected by Mfuzz.

712 **Figure S6. Flow cytometric analysis of lymphocytes, CD3- cells, Related to**  
713 **Figure 4.** 22 samples from 17 LC patients and 30 samples from 17 SC patients were  
714 measured and analyzed. **(A)** Results of lymphocytes, CD3- cells, i.e. P14 (SC) and  
715 P15 (LC). **(B)** Bean plots show the comparison of cell populations between patient  
716 groups. **(C)** Violin plots show cytokines detected by antibody-based flow cytometric  
717 analysis (24 samples from 13 SC patients and 19 samples from 12 LC patients). The  
718 y-axis shows the intensity of each cytokine.

719 **Figure S7. 58 key feature proteins and the expression of top three proteins,**  
720 **ICAM1, FCGR3A and IGKV1-16. Related to Figure 6 (A)** 58 features ranking  
721 according to mean decrease accuracy. **(B)** Protein expression of ICAM1, FCGR3A  
722 and IGKV1-16 between SC and LC groups in discovery dataset test dataset,  
723 respectively.

724

**Figure 1**

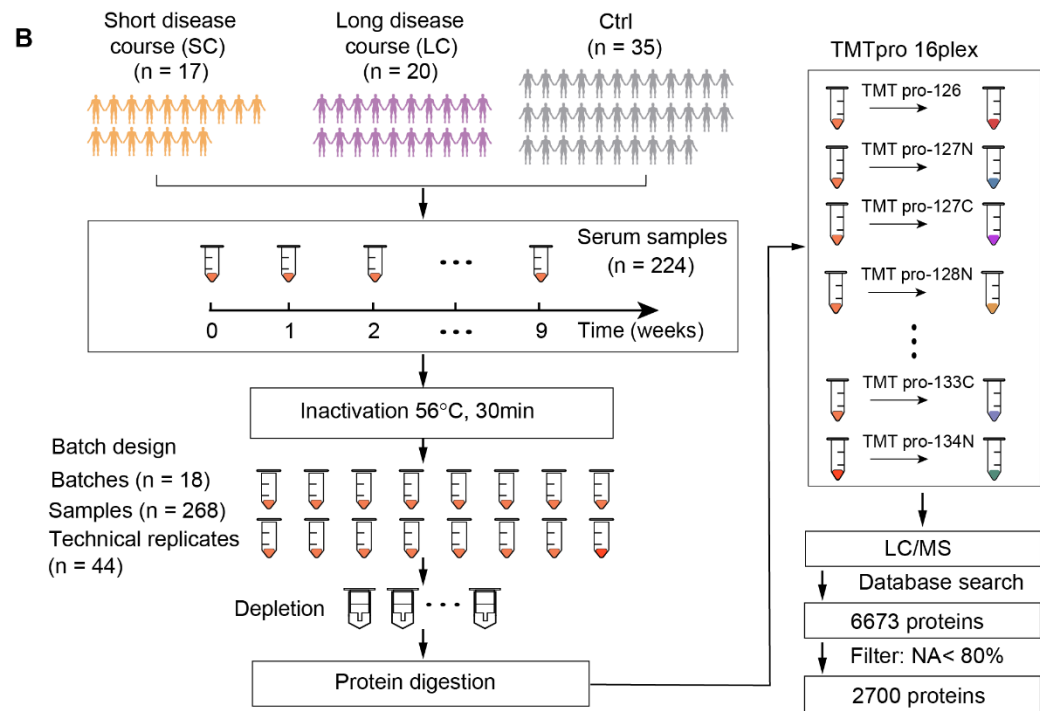
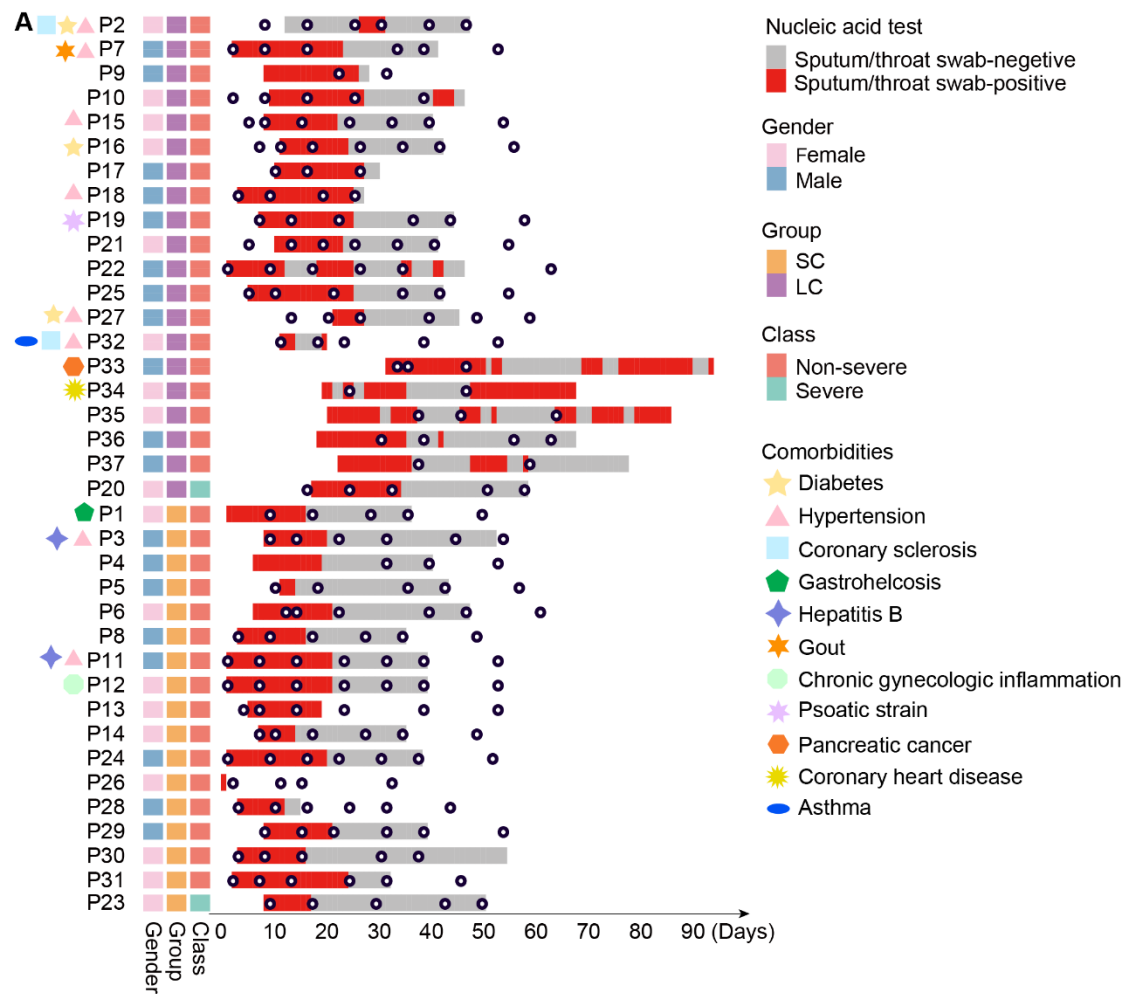


**Figure 2**

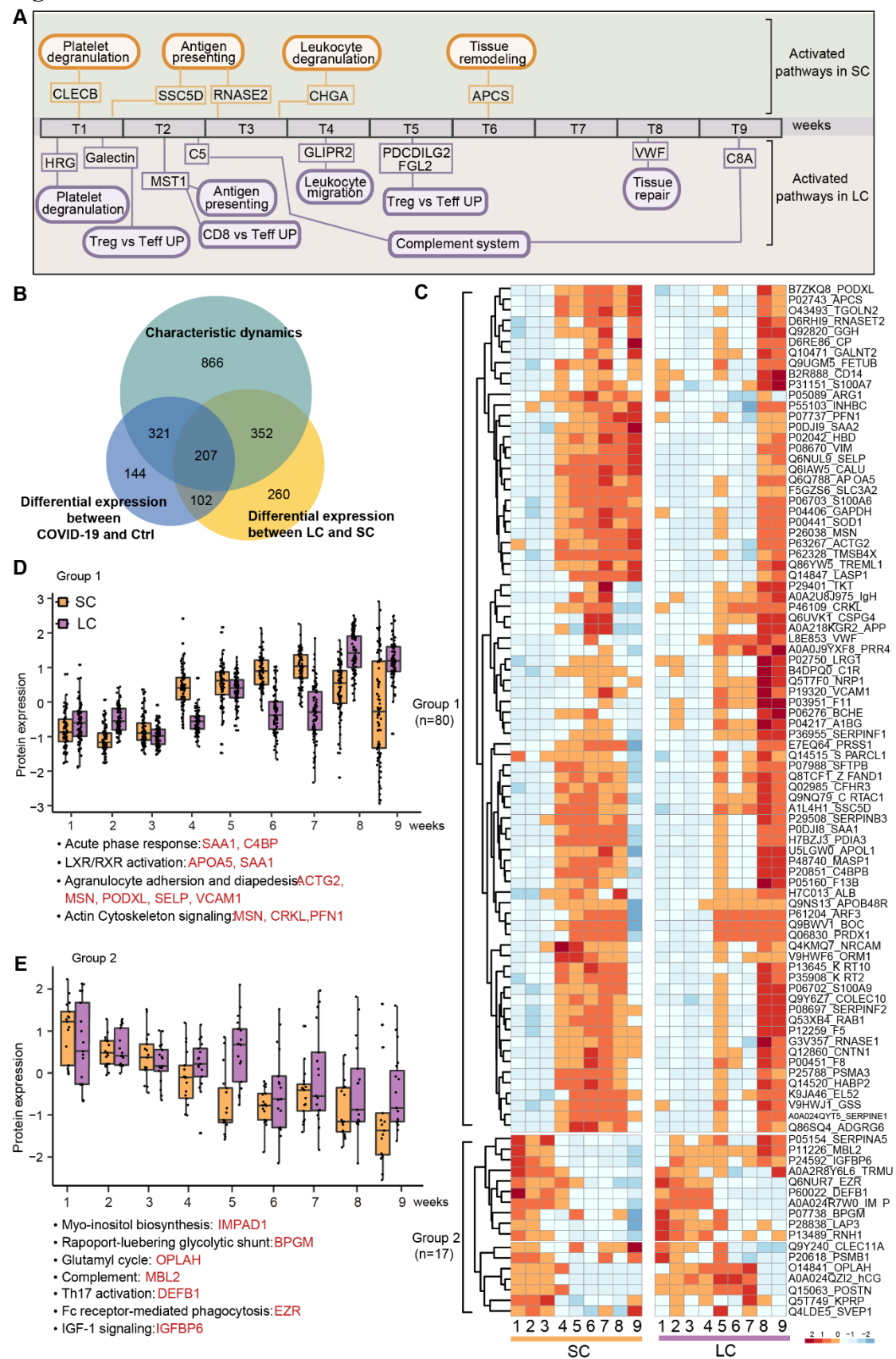




**Figure 3**

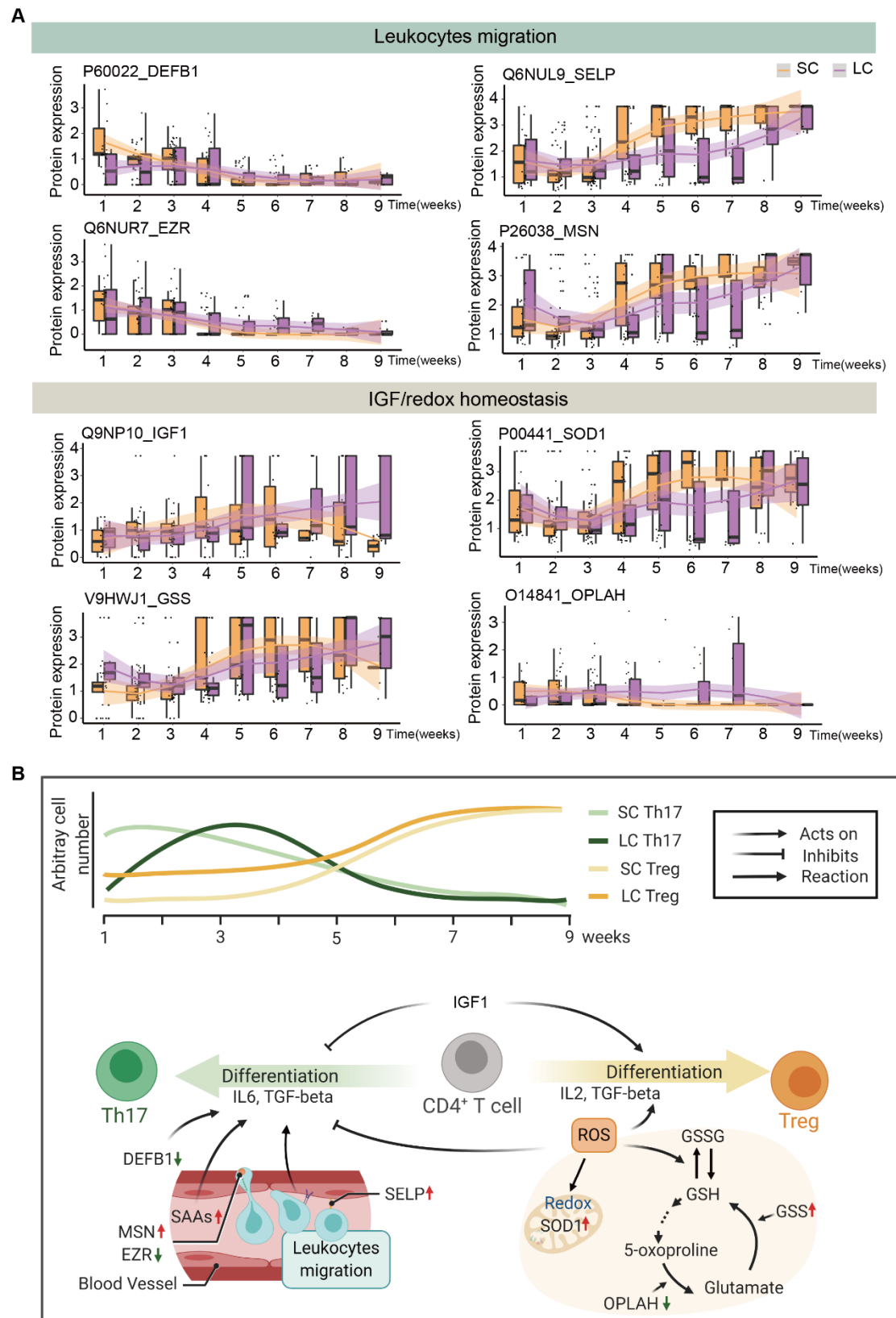


**Figure 4**

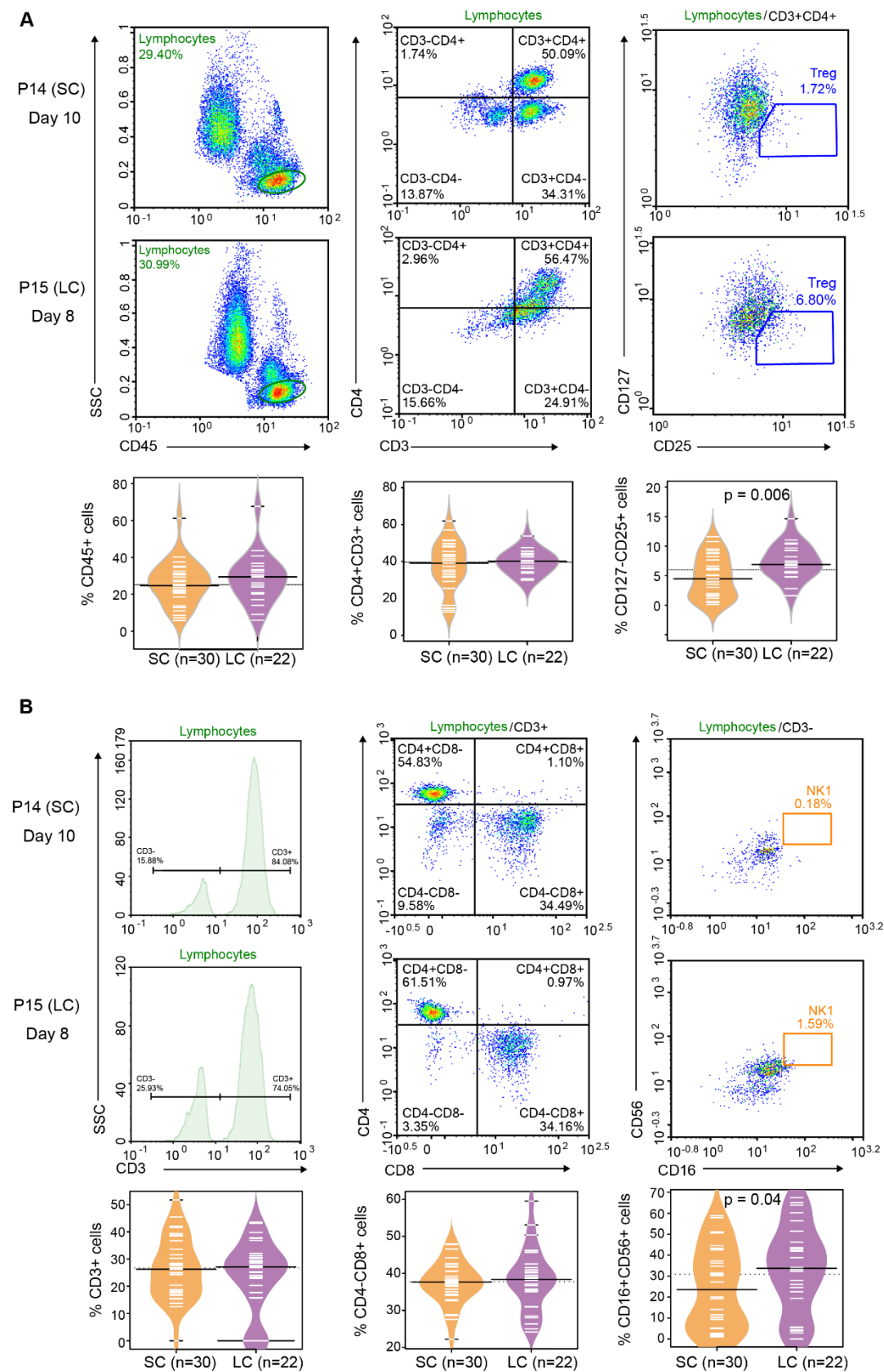
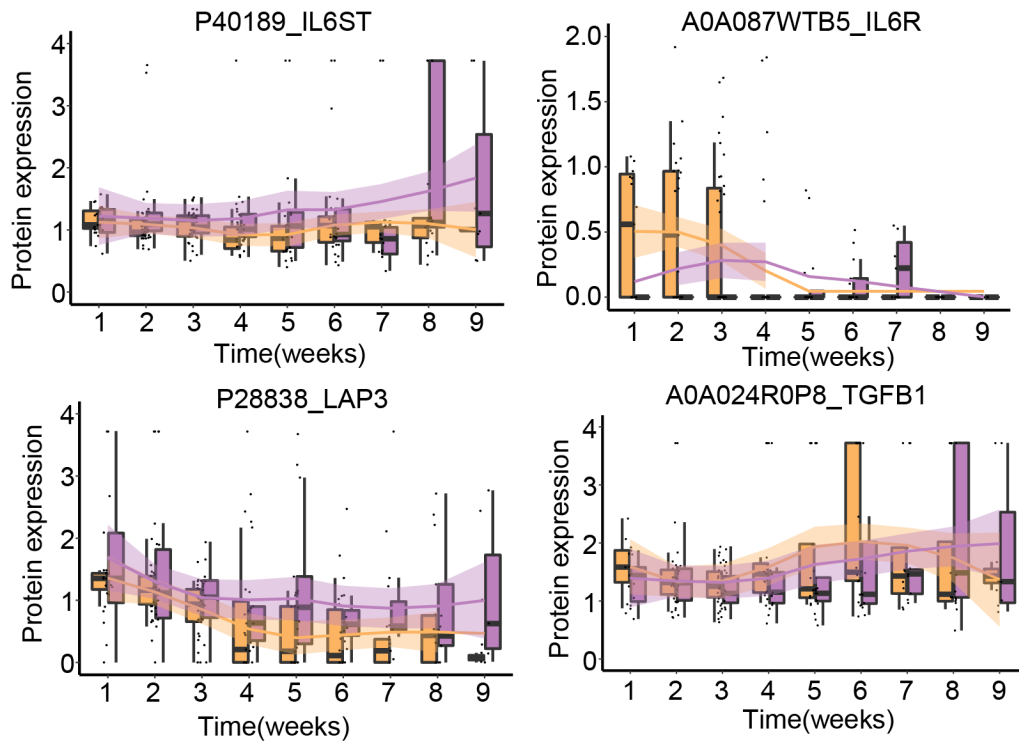


**Figure 5**

**A**



**B**

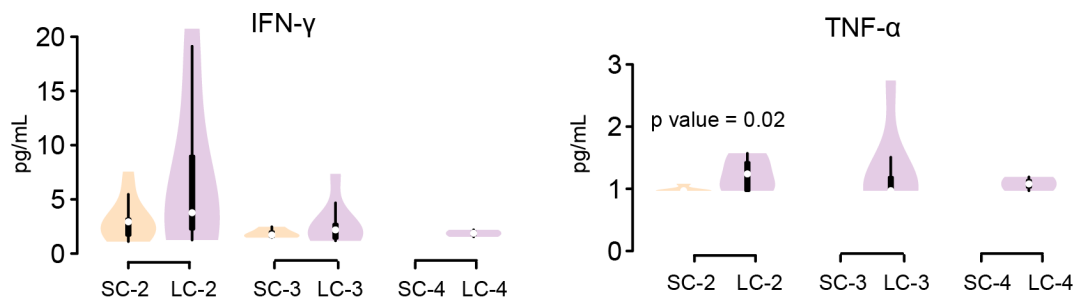


**Figure 6**

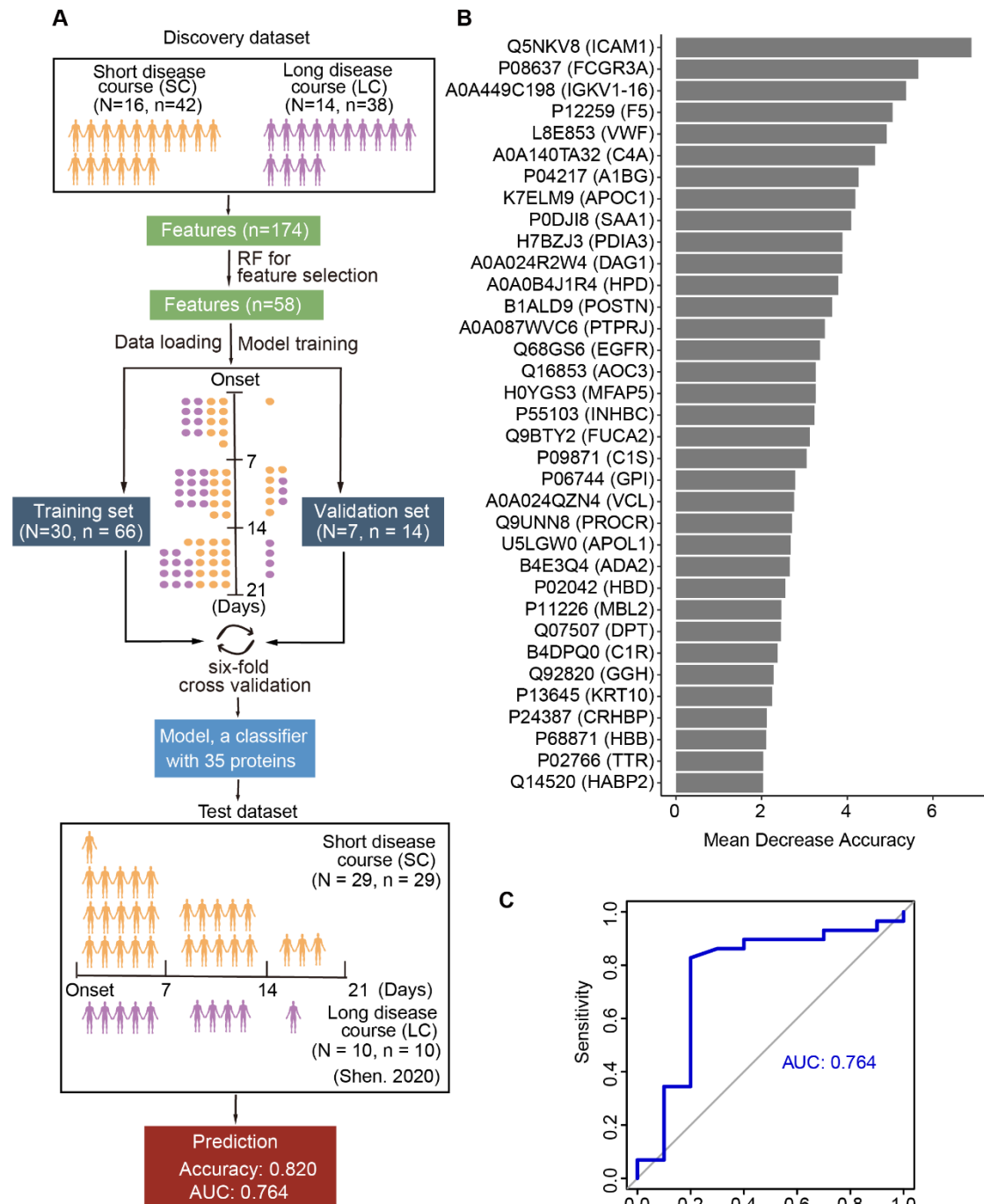


**Figure S1**

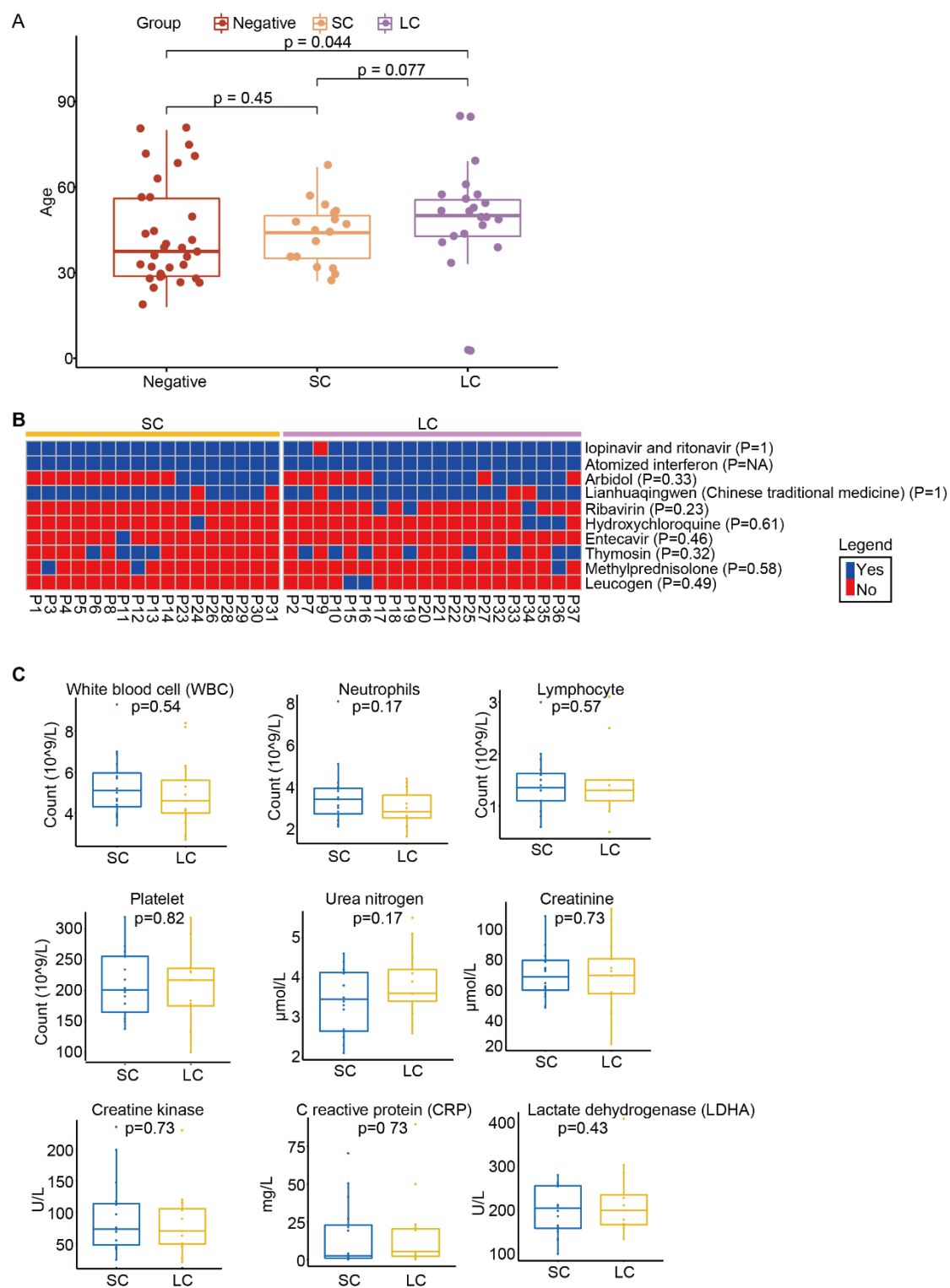


**Figure S2**

A

	B1	B2	B3	B4	B5	B6	B7	B8	B9	B10	B13	B14	B15	B16	B17	B18	B19	B20
126	Pool 1	Pool 1	Pool 1	Pool 1	Pool 1	Pool 1	Pool 1	Pool 1	Pool 1	Pool 1	Pool 1	Pool 2	Pool 2	Pool 2	Pool 2	Pool 1	Pool 1	Pool 1
127C	P23_2	P5_2	P25_1	P29_2	P13_1	P26_1	P7_1	P2_2	P34_4	Pool 2	Pool 2	P10_1B	P22_1B	P23_7	P18_4	P29_5	P26_5	P33_8
127N	P23_3	P5_3	P25_2	P29_3	P13_2	P26_2	P7_2	P2_3	P35_7	P33_7	P2_2B	P10_2C	P22_2B	P23_8	P5_7	P29_6	P28_5	P33_9
128C	P23_5	P9_4	P25_4	P29_4	P13_3	P26_3	P7_3	P27_2	P35_6	P33_5	P2_3B	P10_3B	P22_3B	P20_8	P5_9	P29_8	P28_4	P33_10
128N	P20_3	P17_2	P8_1	P30_1	P10_1	P21_1	P32_2	P27_3	P36_7	P33_6	P2_4B	P10_4	P22_4	P20_9	P8_3B	P30_5	P28_7	P16_4
129C	P20_4	P17_3	P8_2	P30_2	P10_2	P21_2	P32_3	P27_4	P36_5	P10_6	P2_5B	P10_6B	P22_9	P6_6	P25_5	P30_6	P7_5	P16_5
129N	P20_5	P17_4	P8_3	P30_3	P10_3	P21_3	P32_4	P16_1	P37_6	P10_2B	P2_6C	P21_1B	P24_1B	P6_7	P25_6	P15_4	P7_6	P16_6
130C	P6_2	P22_1	P3_2	P18_1	P14_1	P24_1	P1_2	P16_2	Ctrl_1	P2_4	P2_7	P21_2B	P24_2B	P6_9	P25_8	P15_5	P7_8	P16_8
130N	P6_3	P22_2	P3_3	P18_2	P14_2	P24_2	P1_3	P16_3	P2_6	P2_6B	P32_2B	P21_3B	P24_3B	P31_4	P8_4	P15_6	P12_4	P19_6
131C	P6_4	P22_3	P3_4	P18_3	P14_3	P24_3	P12_1	P19_2	P36_7B	P2_5	P32_3B	P21_4	P24_4	P31_5	P8_5	P15_8	P12_5	P19_7
131N	P31_1	Ctrl_5	P11_1	P15_1	Ctrl_12	P28_1	P12_2	P19_3	P7_3B	Ctrl_2B	P32_4B	P21_5	P24_5	P31_7	P8_7	P13_4	P12_6	P19_9
132C	P31_2	Ctrl_16	P11_2	P15_2	Ctrl_35	P28_2	P12_3	P19_4	P18_2B	Ctrl_6B	P32_6	P21_6	P24_6	P35_9	P11_4	P13_6	P12_8	P2_2C
132N	P31_3	Ctrl_32	P11_3	P15_3	Ctrl_34	P28_3	Ctrl_18	Ctrl_30	P22_3B	Ctrl_26B	P32_8	P1_5	P24_8	P36_8	P11_5	P13_8	P9_5	P4_6
133C	Ctrl_6	Ctrl_27	Ctrl_3	Ctrl_4	Ctrl_22	Ctrl_10	Ctrl_11	Ctrl_23	Ctrl_14	P21_3C	Ctrl_6B	P1_6	P3_5	P36_9	P11_6	P14_4	P12_3B	P4_8
133N	Ctrl_13	Ctrl_17	Ctrl_24	Ctrl_25	Ctrl_29	Ctrl_36	Ctrl_8	Ctrl_9	Ctrl_15	P25_4B	Ctrl_13B	P1_8	P3_7	P20_5B	P11_8	P14_5	P37_9	P22_5
134N	Ctrl_31	Ctrl_33	Ctrl_26	Ctrl_21	Ctrl_7	Ctrl_19	Ctrl_28	Ctrl_20	Ctrl_1B	P19_4B	Ctrl_31B	Ctrl_27B	P3_8	P10_3C	P5_6	P14_7	P34_7	P16_2B

B

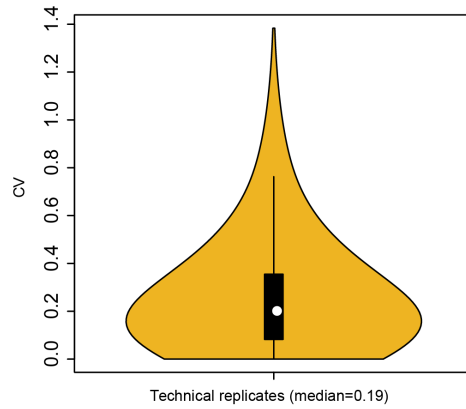
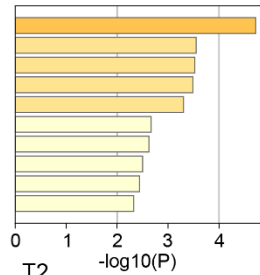




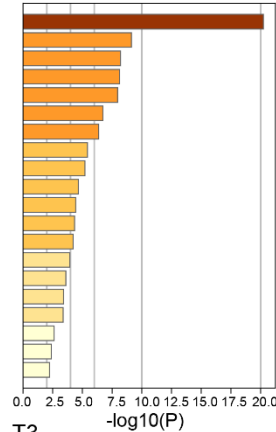
**Figure S3**

T1



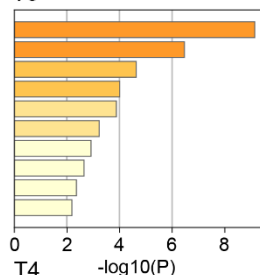
- R-HSA-114608: Platelet degranulation
- M5885: NABA MATRISOME ASSOCIATED
- GO:0050830: defense response to Gram-positive bacterium
- GO:0008285: negative regulation of cell proliferation
- R-HSA-381426: Regulation of Insulin-like Growth Factor (IGF) transport and uptake by Insulin-like Growth Factor Bi
- GO:0006575: cellular modified amino acid metabolic process
- GO:0006979: response to oxidative stress
- M3468: NABA ECM REGULATORS
- GO:0045926: negative regulation of growth
- GO:0098742: cell-cell adhesion via plasma-membrane adhesion molecules

T2



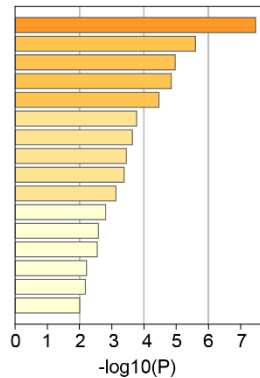
- R-HSA-166658: Complement cascade
- GO:0019882: antigen processing and presentation
- GO:0045055: regulated exocytosis
- GO:0019730: antimicrobial humoral response
- R-HSA-114608: Platelet degranulation
- R-HSA-140877: Formation of Fibrin Clot (Clotting Cascade)
- GO:0030198: extracellular matrix organization
- R-HSA-381426: Regulation of Insulin-like Growth Factor (IGF) transport and uptake by Insulin-like Growth Factor Bi
- GO:0005996: monosaccharide metabolic process
- GO:0031589: cell-substrate adhesion
- hsa05150: Staphylococcus aureus infection
- GO:1901136: carbohydrate derivative catabolic process
- GO:0051701: interaction with host
- hsa04514: Cell adhesion molecules (CAMs)
- M14532: ST PHOSPHOINOSITIDE 3 KINASE PATHWAY
- R-HSA-948021: Transport to the Golgi and subsequent modification
- GO:1901658: glycosyl compound catabolic process
- GO:0090288: negative regulation of cellular response to growth factor stimulus
- GO:0008285: negative regulation of cell proliferation
- GO:0006935: chemotaxis

T3



- GO:0043299: leukocyte degranulation
- GO:0050918: positive chemotaxis
- GO:0043588: skin development
- GO:0006959: humoral immune response
- GO:0019882: antigen processing and presentation
- hsa04610: Complement and coagulation cascades
- R-HSA-6807878: COPI-mediated anterograde transport
- GO:0019932: second-messenger-mediated signaling
- GO:0030203: glycosaminoglycan metabolic process
- GO:0009566: fertilization

T4



- GO:0002576: platelet degranulation
- hsa04145: Phagosome
- GO:0030335: positive regulation of cell migration
- R-HSA-166658: Complement cascade
- GO:0006959: humoral immune response
- GO:0034764: positive regulation of transmembrane transport
- GO:0016339: calcium-dependent cell-cell adhesion via plasma membrane cell adhesion molecules
- GO:0030198: extracellular matrix organization
- GO:0032355: response to estradiol
- GO:0019226: transmission of nerve impulse
- hsa04974: Protein digestion and absorption
- R-HSA-8957275: Post-translational protein phosphorylation
- M5885: NABA MATRISOME ASSOCIATED
- GO:0052547: regulation of peptidase activity
- GO:0005996: monosaccharide metabolic process
- GO:0048469: cell maturation

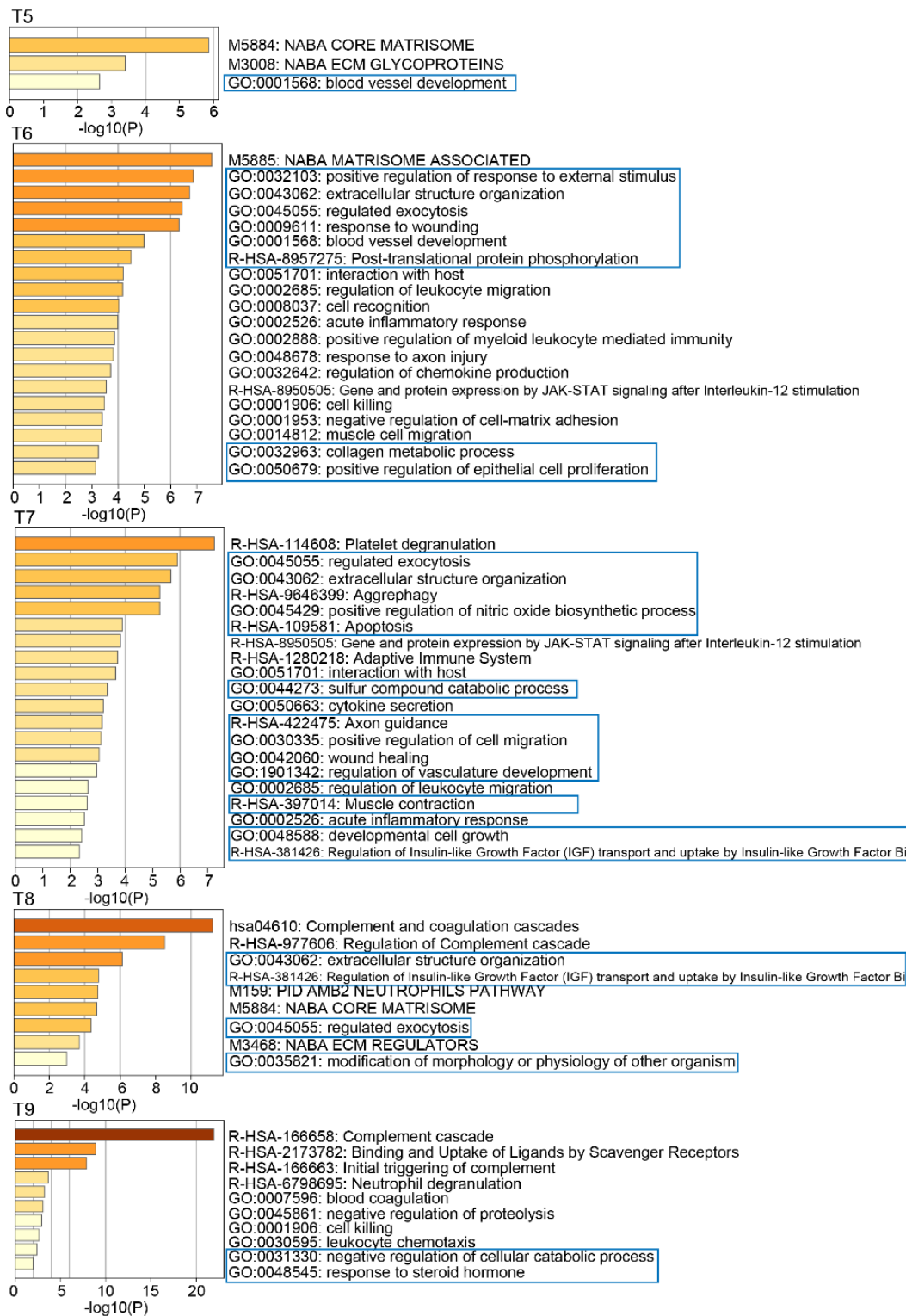
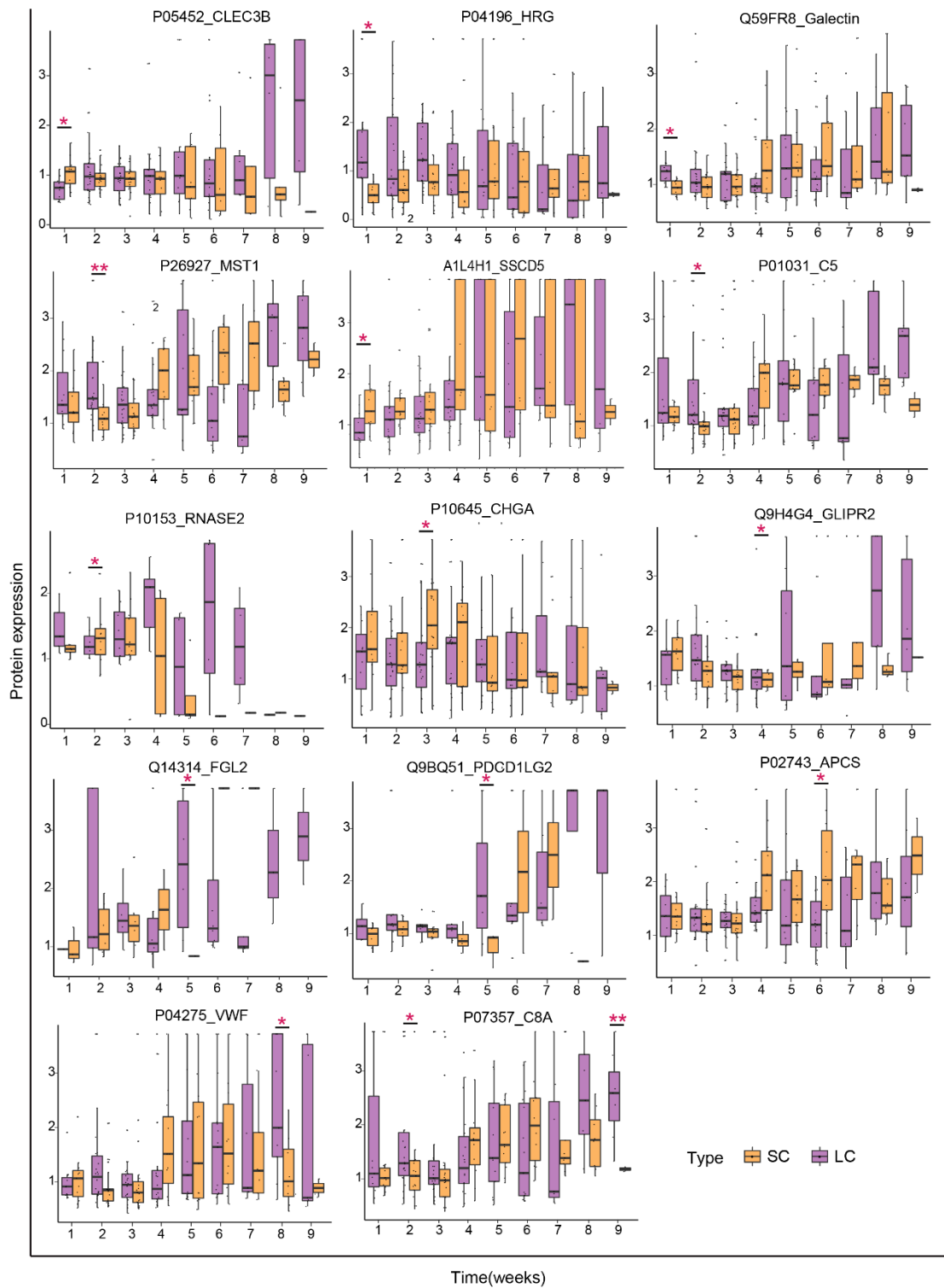
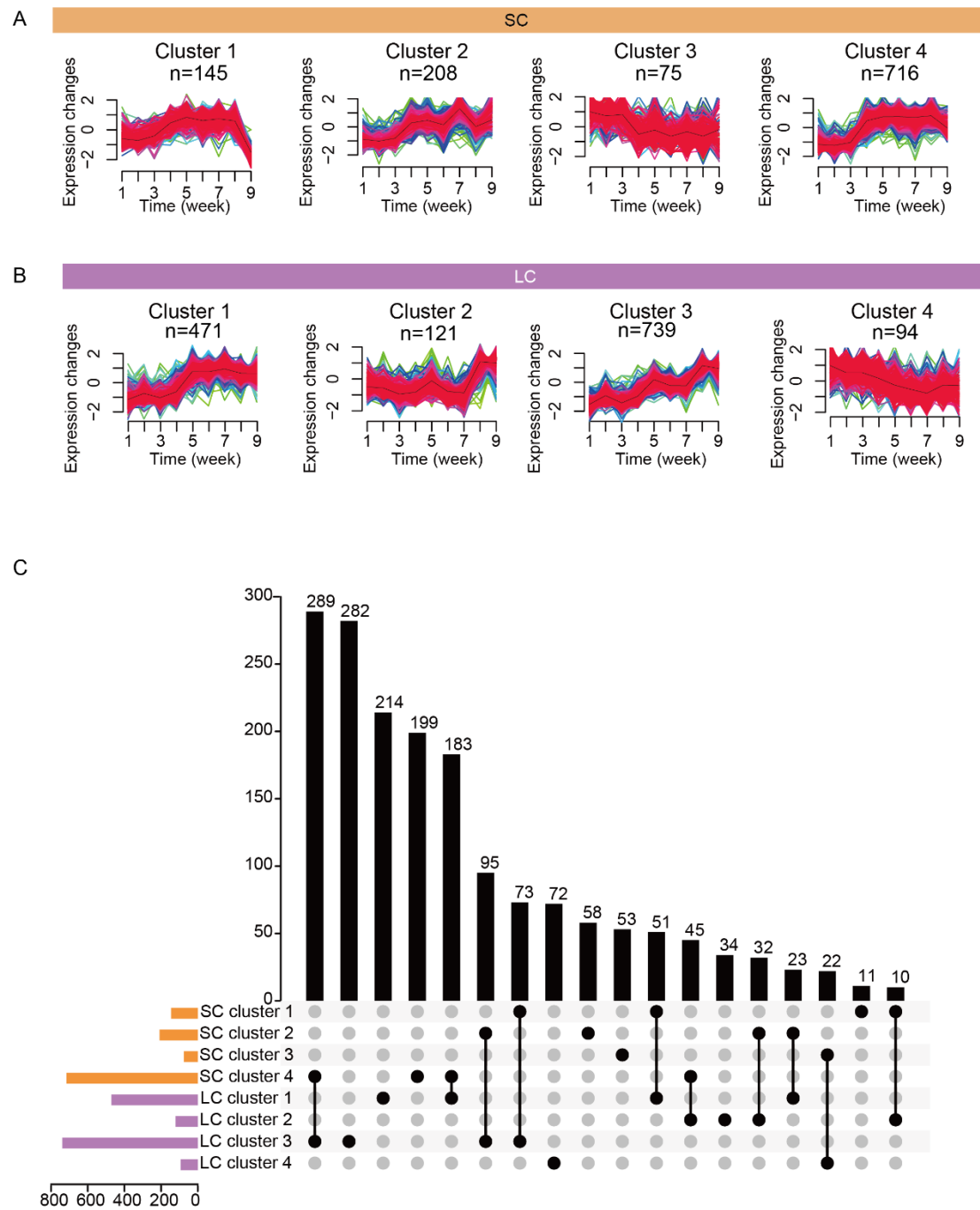


Figure S4



**Figure S5**



**Figure S6**

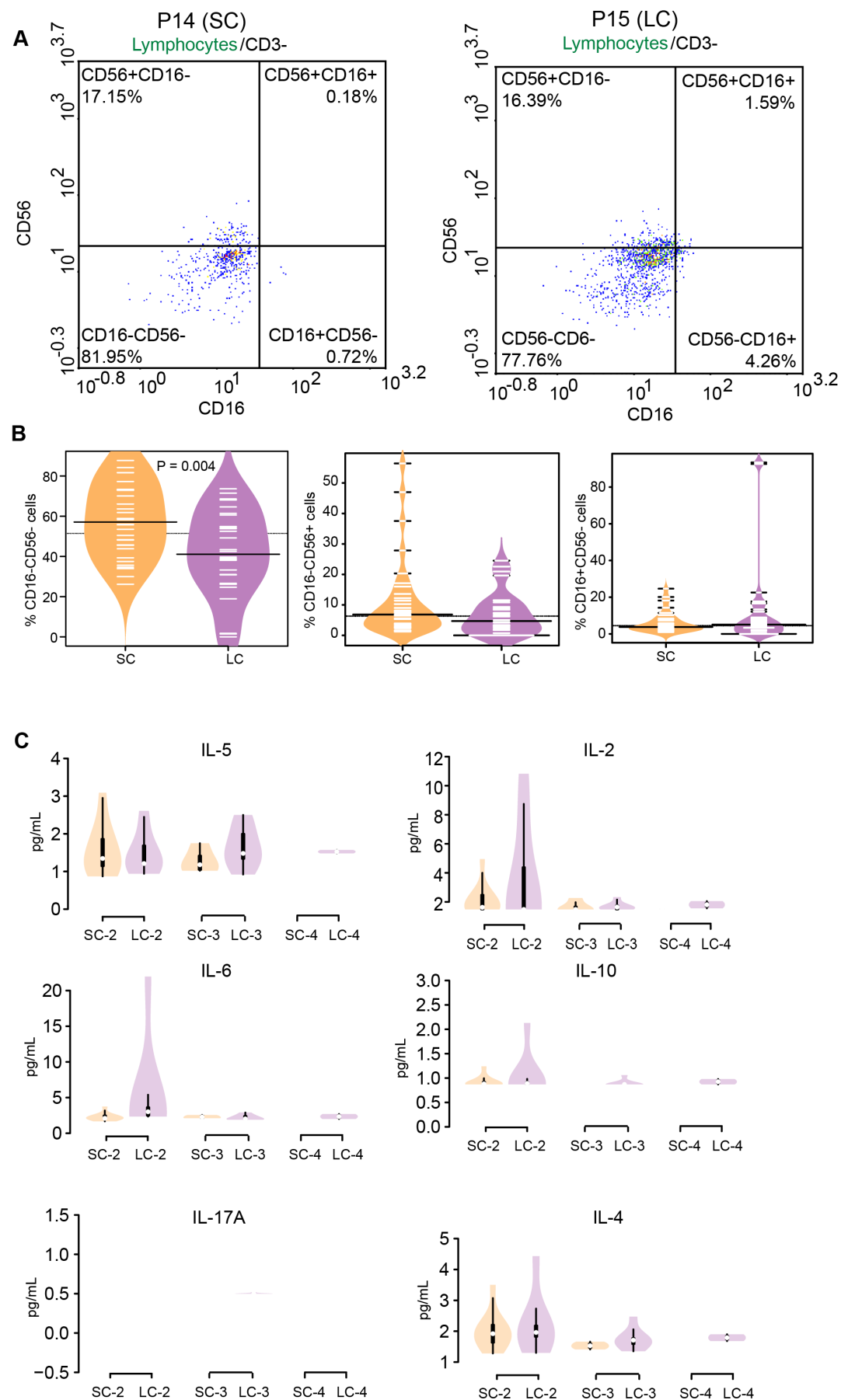
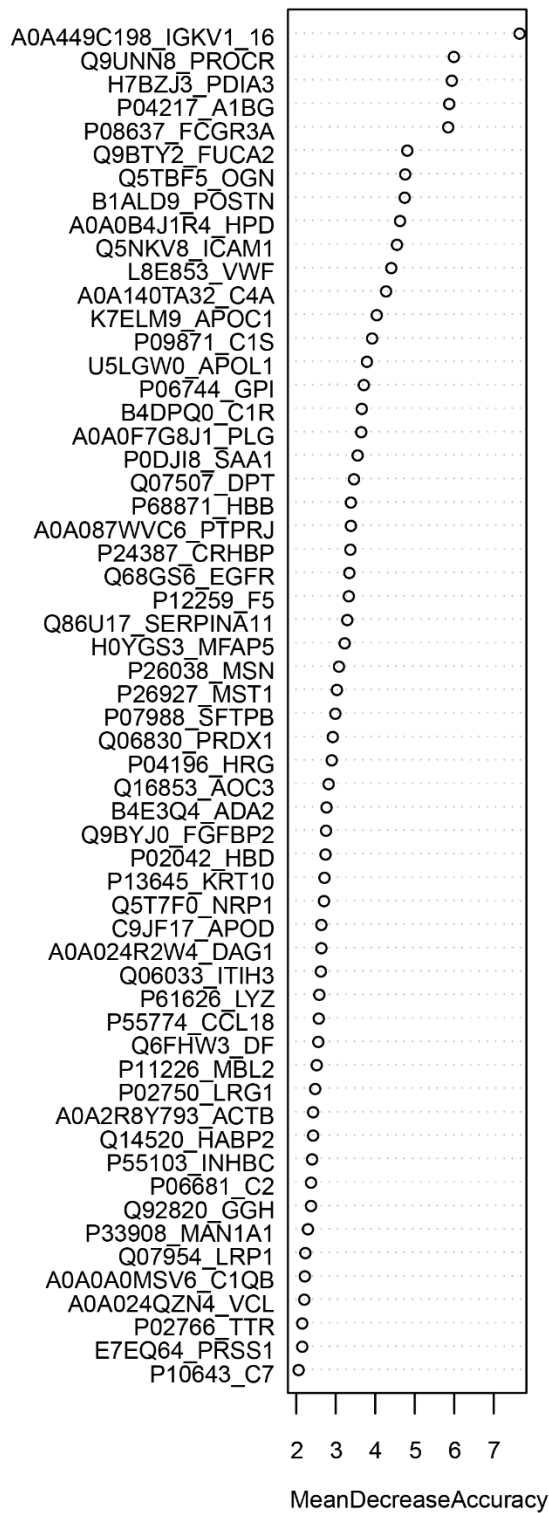


**Figure S7**

**A**



**B**

